Paper submitted to the International
Conference on Elementary Particles
held at Sienna from 30th September
to 5th October 1963

NPA/Int. 63-20
Meyrin, 17th September 1963

THE EXTRACTED 25 GEV/C PROTON BEAM FOR THE CERN NEUTRINO EXPERIMENT

by

R. Bertolotto, H. van Breugel, L. Caris, E. Consigny, H. Dijkhuizen,
J. Goni, J.J. Hirsbrunner, B. Kuiper, B. Langeseth, S. Milner, S. Pichler,
G. Plass, G. Pluym, H. Wachsmuth and J.P. Zanasco.

(Presented by G. Plass)

Summary : The 25 GeV/c proton beam is extracted from the CERN proton synchrotron within a time-interval of 2.1 μs. For the production of a high flux of pions and kaons the beam is then guided towards an external target and in the target focused to approx. 1 mm^2 cross section. Results of preliminary beam studies are discussed and the apparatus used described.

1. Introduction

It became clear soon after the first proposals for experiments with neutrinos from high energy accelerators were made that an extracted beam of high energy protons would combine a number of properties of interest for such experiments, such as :

1) the small emittance of the circulating proton beam could be essentially preserved. It permits focusing of the beam to a small diameter in a long and thin target and hence an efficient use of the accelerated protons;

2) the time structure : the total burst length of a fast ejected beam would be convenient for bubble chambers. The bunch structure permits further gating of counters or spark chambers to a ratio of 10^7 : 1 against cosmic rays and time of flight rejection of slow neutron background.

In fact the rates from internal targets of less than one useful event per day and ton of detector realized at the Brookhaven A.G.S. [1] or expected at the CERN P.S. [2), 3), 4)] were marginal for doing neutrino experiments with justifiable amounts of machine time, and the feasibility was largely dependent on the geometry of the synchrotron magnet. Considerations about the use of the then planned fast ejected proton beam for the C.P.S. [5] led to the proposal of a "magnetic horn" [6),7),8)] for directing the pions originating from an external target towards the detector of the neutrino induced interactions. This device was expected to increase the rate to several events per day in the CERN heavy liquid chamber without substantially changing the existing proposals for the experimental layout [3), 9)] from which the present arrangement was developed.

The external proton beam has up to date delivered in about 35 days of running approx. 10^6 pulses mainly of 24.6 GeV/c protons onto the external target. The accelerated intensity was mostly between 7 and 8.10^{11} protons per pulse of which more than 90 o/o were ejected. The beam worked satisfactorily after little setting-up and testing time and the neutrino experiment was started immediately. There was little time available for systematic studies of the beam ; the presented data on the beam properties are hence preliminary.

2. Description of the beam

2.1 Trajectory

The layout of the final experimental set-up is shown in Fig. 1. The experiment has been arranged such as to take up the minimum space in the P.S. South Hall, i.e. the detectors have been placed into the North West corner of this hall, leaving place for most of the other standard beams derived from internal targets. As a consequence, the extracted proton beam could not be used within the range of directions provided by the ejector magnet (hatched cone in Fig. 2), but has been further deflected to follow closely the P.S. ring magnet.

Fig. 2 shows a layout of the extraction equipment and the external beam. The proton beam is ejected from the synchrotron by exciting a betatron amplitude of 20 mm with the fast kicker magnet, and by a subsequent 24 mrad outward deflection by the septum magnet. After having left the machine field, it is deflected into the direction of the detectors (passing at the same time clear behind the yoke of the P.S. magnet unit 4) by a deflection of 101.5 mrad towards the machine centre, which is accomplished by 5 pulsed magnets of approximately equal strength. A vertical correction of 0.15 mrad is provided by a sixth small magnet.

The trajectory of the ejected beam through the P.S. magnet up to the point at which it emerges from the P.S. stray field has been traced with a computer programme [10]. This integrates the equation of motion in small steps, the field values being interpolated from a measured field table [11]. Fig. 3 and 4 show the trajectory through the P.S. magnet units in more detail ; also shown i the result of a trajectory measurement in the last magnet unit (Fig. 4). The outward parallel displacement of the measured curve corresponds to approx. 1.5 mm error in the relative alignment between the septum magnet and the measuring equipment. This is within the expected overall measuring precision.

The machine vacuum is terminated one magnet unit downstream from the septum magnet. From then on the beam travels in a vacuum tube, mostly a 40 mm outer diameter plexiglass tube, at a rough vacuum of approx. 3 Torr. The remaining r.m.s. Coulomb scattering angle is smaller than 0.02 mrad. That the beam is well centered in the vacuum tube can be inferred from Fig. 5 where the spots obtained by introducing photographic paper directly into the vacuum tube are reproduced. For an explanation

of the small satellite spot visible in two places see par. 3.1.

2.2 Beam optics

The fields in the two ejection magnets are sufficiently constant in space and time to have only a small influence on the beam properties. The effect is negligible for present purposes.

The beam leaves the linearized field region of the P.S. aperture in the magnet units downstream from the septum magnet, where the location of the ejected beam with respect to the pole faces is indicated in Fig. 4. It traverses a horizontally focusing field in one and horizontally defocusing fields in three half magnet units with mean gradients at 24.8 GeV machine energy of approx. 4.2 Wb/m^3 in the first and 4.3 Wb/m^3, 2.1 Wb/m^3 and 1.3 Wb/m^3 respectively in the other sections. The resulting horizontally defocusing effect is compensated by inserting a horizontally focusing quadrupole (Q1 in Fig. 2) between the two magnet units. A beam of less than 0.5 mrad divergence is thus produced (cp. Fig. 5).

The beam is then focused to very small size by a quadrupole triplet (Q_2 - Q_4 in Fig. 2). The lens strengths as computed with another standard programme [12] are displayed in Fig. 6. Fig. 7 shows the spots obtained on Polaroïd film when the lenses are tuned so as to produce a focus in the space between the deflection magnet B 6 and the horn. Fig. 8 has been obtained by inserting at the same place photographic paper longitudinally into the beam in horizontal and vertical planes.

The obtained spot sizes depend on the sensitivity of the photographic material and are in fact too large due to secondary particles. As typical examples G 5 and K - 1 emulsions exposed to $1.6 \cdot 10^{10}$ protons are shown in Fig. 9. The large black spot in Fig. 9 a is seen to be almost entirely due to radial tracks of secondaries, and the actual beam cannot be distinguished. The total doses have been obtained in different ways in Figs. 9 b, c and d which thus give an indication of the stability of the system at least during short periods. In order to obtain a better estimate of the beam size a series of K - 1 emulsions has been exposed to doses between $3.5 \cdot 10^8$ and $1.6 \cdot 10^{11}$ protons and again all plates are overexposed in the centre. However, by plotting constant blackening against radius (using a rather subjective criterion of blackness in microscopic observation) a curve as in Fig. 10 can be obtained. Though the peak of the curve is unknown, it allows the conclusion

that more than 90 o/o of the beam are contained in dimensions smaller than 0.8 mm in horizontal and 1.3 mm in vertical directions.

It can be inferred from Fig. 4 that the beam avoids the regions of strongest nonlinearity of the synchrotron field and that phase-space should hence be essentially conserved. Phase-space ellipses in the horizontal plane have been constructed by tracing with the computer a number of trajectories with initial conditions lying on an assumed machine phase-space ellipse. The resulting contours are shown in Fig. 11.

An approximate emittance value of an ejected beam of $1.5 \cdot 10^{10}$ protons has been estimated from Fig. 10 and similar exposures at the end of lens Q 4. The result is shown in table 1. The acceptance of the circulating beam is computed from the horizontal beam dimension which is approximately determined by letting the ejection magnet intercept the beam.

Table 1

Extracted beam emittance

	measured emittance	estimated emittance of the circulating beam
horizontal	$7 \pi \cdot 10^{-7}$ rad . m	$4 \pi \cdot 10^{-7}$ rad . m for beam width 6 mm
vertical	$3 \pi \cdot 10^{-7}$ rad . m	

2.3 Efficiency

The bunch structures of the circulating and the ejected beam as observed with electrostatic pick-up electrodes are shown in Fig. 12. The loss of the second bunch and occasional mutilation of the first in the ejected beam are due to a temporary deficiency of a storage line of the ejection system (see par. 3.1). Since normally no beam is left in the machine and there is no evidence for losses in the external beam, (cp. Fig. 5), we infer that the extraction efficiency is at present between 90 and 95 o/o. This is in agreement with the indication of a calibrated beam current transformer in the external beam path.

The stability of the whole system is such that 98 o/o of the ejected pulses pass through a 2.5 mm diameter hole in a fluorescent screen mounted in front of the 4 mm diameter target without significant light production.

3. Apparatus and instrumentation

3.1 Fast beam extraction

The beam is extracted in two stages (see Fig. 3). A sudden distortion induced by the "kicker" magnet in the synchrotron orbit makes the beam pass through the aperture of a second magnet (bending magnet in Fig. 3) which deflects it out of the synchrotron magnet field. For maximum efficiency the kicker magnet field rises between the passage of two subsequent bunches of the circulating proton beam (i.e. in 100 ns) to approx. 0.1 Wb/m^2 and stays constant for the revolution time of the synchrotron of 2.1 μs (Fig. 13). It yields 1 mrad deflection and some 20 mm amplitude of the orbit distortion. The bending magnet must have low leakage field in order not to distort the synchrotron orbit before ejection, because its field rises more slowly and to a higher value. It rises to 1 Wb/m^2 in 75 μs and deflects the beam through 24 mrad angle out of the machine. The pulse of the kicker magnet is synchronized to the top of the sinusoïdal pulse (top trace in Fig. 14) which is sufficiently flat during the 2.1 μs interval within which the beam is ejected.

Both magnets are located inside vacuum tanks and cover in their working positions part of the P.S. vacuum aperture. Since the beam fills a large part of the vacuum chamber at low energies the ejection magnets are moved into their positions

in each acceleration cycle after the betatron oscillations have been sufficiently damped and the beam diameter is smaller than 1 cm. The magnets are shown in their vacuum tanks and the hydraulic actuators are indicated in Figs. 15 and 16.

In order to obtain the required trapezoïdal field pulse shape, the kicker magnet is pulsed in a matched transmission line circuit [13), 14)] of 10 ohm impedance as schematically represented in Fig. 17. A lumped element transmission line (LSL and SSL) is charged to a certain voltage. Upon closing the gap G a voltage wave of half the charging voltage with the associated current wave travels down the circuit through the magnet, the energy finally being dissipated in the terminating resistor R. The charged line consists of two parts, one for pulses of 100 ns duration (SSL) and one for 2.1 μs (LSL) pulse duration which permit respectively the ejection of single bunches or of the total beam. A mismatch of the 100 ns storage line in the first assembly explains the departure from trapezoïdal pulse shape in Fig. 13, the existence of the second spot in Fig. 5 (due to the bunch deflected by the first peak of the pulse) and the missing bunch in Fig. 12 which falls into the subsequent minimum.

The pulse generator assembly is shown in Fig. 18. The whole system has been designed coaxial, the outer conductor always being connected to ground potential. The rack contains from top to bottom the 2.1 μs storage line, a high voltage switch, the 100 ns storage line, the three electrode "swinging cascade" type spark gap [17)], and a mutual inductance for observation purposes. Five 50 ohm cables in parallel guide the pulse to the magnet and further to the oil-cooled resistor assembly.

The kicker magnet consists of two units (Figs. 19 and 20) of coaxial structure the outer conductor of course being interrupted to open the magnet gap. Ferrite rings with an air gap are located between the inner and outer conductors and the impedance is matched by circular plate capacitors located between the ferrite rings. The whole magnet is sealed vacuum tight and is oil-impregnated to improve the high voltage reliability. The radial field distribution in the gap is shown in Fig. 21. Some parameters and ratings of the kicker magnet and its circuit are collected in table 2.

A low leakage field is achieved by a "septum" type magnet structure, where the return current conductor ("septum") is so placed that it closes the magnet gap. The septum magnet (Fig. 22) consists of two units in series each built up of blocks of glued Si-steel plates and is excited by a single -turn winding. It is

pulsed in order to ease the problems of cooling the heavily loaded septum conductor. Eddy currents induced by the pulse in the front plate that cools and retains the septum at the same time reduce somewhat the leakage field. The radial field distribution in the gap and the leakage field outside the septum are shown in Figs. 23 and 24.

Fig. 25 shows the "delayed crowbar" pulsing circuit of the septum magnet. The capacitor is first discharged through the ignitron pair S and the magnet (Fig. 14, top trace). The discharge would continue ringing, but before the reverse voltage reaches its peak the capacitor is rapidly discharged through the ignitrons CS and the low inductance damping resistors DR dissipate the stored energy. (Fig. 14 lower trace). In Fig. 26 the low inductance arrangement of the pulser circuit is shown. Parameters and ratings of the bending magnet and its circuit are given in table 3.

A first outline of the fast ejection system has been presented in ref. 5 and a more detailed account of the completed installation in ref. 16.

3.2 Beam transport

In order to deflect the beam into the chosen place for the detectors and at the same time to produce a focus near the machine the beam transport components had to be located very near the synchrotron magnet. This requirement limits their external dimensions, while the small size of the beam allows for small apertures. The deflection fields and the gradients have been planned for very high values in order to reduce the required lengths. The associated power problem in the restricted space can be coped with by pulsing all these magnets, since the fast ejected beam has only 2 μs pulse duration.

There are four types of magnet components, short and long window frame bending magnets and short and long quadrupoles with hyperbolic pole pieces. They are all made from low carbon steel laminations and excited by several turns of water cooled copper conductor cast in epoxy resin. The different components are shown in Fig. 27 and 28 and their relevant dimensions are included in table 4. The field distribution in the deflection magnets is shown in Fig. 29 and the variation of the gradient in the quadrupoles is represented in Fig. 30. The pole profile of the quadrupoles favours the high gradients.

The beam transport components are pulsed from circuits such as shown in Fig. 31. The capacitor is discharged into the magnet coil through ignitron 1. The ringing frequency of the circuit is such as to allow the ignitron to extinguish after one half cycle, leaving the capacitor charged with reversed polarity. The capacitor polarity is subsequently returned to the initial sense via ignitron 2, recovering approx. 35 o/o of the initial voltage. Extinguishing of the ignitrons is ensured by the saturable reactor. The frequencies of the circuits for the various magnets (see table 4) vary according to the inductance of the magnetic components and according to the required current within the limit imposed by the requirement of ignitron exstinction. Standardized capacitor units can thus be used, the supply voltages being the same within certain limits. The capacitors are charged by transductor controlled supplies [17] which are stable to better than 0.1 o/o.

The main parameters of the beam transport magnets and the pulsing circuits are listed in table 4. The installed beam transport magnets are shown in Figs. 32 and a pulser rack in Fig. 33. A more detailed description of the beam transport equipment is given in ref. 18.

3.3 Beam observation and monitoring

The essential properties of this beam - densities of the order of 10^{11} p / mm^2 in space and 3.10^{18} p / s in time - render impossible the use of detection methods relying on the identification of single particles. The following techniques are therefore used for beam observation purposes :

- fluorescent screens for beam alignment adjustment and monitoring ;
- a toroïdal transformer for intensity monitoring ;
- electrostatic pick-up electrodes for time - structure (bunch number) observation ;
- photographic material of various kinds (normal copying paper, Polaroïd material, nuclear emulsions) are used for special purposes as described in par. 21 and 22.

Normal ZnS fluorescent screens viewed by television cameras have been the main tool for observing the ejected beam [19]. Spaces for screens and their pneumatic or electromagnetic drives have been provided in the places marked in Fig. 2. Most of them served in the setting-up period, but only two are essential for the continuous

monitoring of the beam. A window frame screen around the aperture of the septum magnet is used to monitor the position of the circulating synchrotron beam relative to the ejection equipment since the beam position and diameter have a tendency to vary slowly. Another screen, with a 2.5 mm diameter hole in the centre, is mounted onto the target holder of the magnetic horn and aligned with the target. Normally, the beam will pass through the hole and hence hit the target.

The beam current transformer is of a type similar to that used for the measurement of the circulating beam intensity and has been described elsewhere [20]

An electrode placed near the beam typically produces an electrostatic pick-up voltage up to 1 V. It yields direct information on the beam bunch structure. A system of four electrodes placed around the beam is being made as an alternative for beam position monitoring.

The standard P.S. displays of radial beam position, trapped proton intensity (digital indication at preselected machine energies), and of the variation of the proton intensity during the acceleration cycle complete the necessary set of monitoring equipment.

4. Acknowledgements

We gratefully acknowledge the contributions of B. de Raad who worked out the first designs of the external beam [7), 19)] and of D.A.G. Neet who initiated the design of most of the electronic equipment of the ejection system [21)] and the external beam [17)]. We wish also to thank Dr. C.A. Ramm for his stimulating support of this work. We are indebted to the Vacuum Group of the M.P.S. Division who have provided the vacuum tanks and special chambers for the ejection system and to the members of the Apparatus Layout Group for their willing cooperation in the installation and alignment of our equipment. The sustained struggle of the M.P.S. operating staff to combine maximum intensity with stable machine conditions was as important as Dr. H.G. Hereward's kind help during the running-in sessions. Finally, we thank the members of the ENG Drawing Office and of the CERN workshops as well as all the members of the N.P.A. Division who have been involved in the project for their untiring effort.

/fv

Distribution : (open) PS/4013
Scientific staff of N.P.A.

References

1) G. Danby et al. - Observation of high energy neutrino reactions and the existence of two kinds of neutrinos, Phys. Rev. Letters 9, 36 (1962)

2) G. Bernardini - The programme of neutrino experiments at CERN, Proc. Int. Conf. on High Energy Physics, Rochester, 1960

3) F. Krienen, R. Salmeron, J. Steinberger - Proposal for an experiment to detect neutrino induced interactions, CERN - PS/Int. EA 60-10 (1960)

4) G. von Dardel - Counting rate in the planned experiment to detect neutrino induced interactions, CERN-NP/Int. rep. 61-5

5) B. Kuiper, G. Plass - On the fast extraction of particles from a 25 GeV proton synchrotron, CERN 59-30

6) S. van der Meer - A directive device for charged particles and its use in the enhanced neutrino beam, CERN 61-7

7) S. van der Meer, B. de Raad - Proposal for an enhanced neutrino beam, CERN-NP/Int. 61-3

8) M. Giesch et al. - Status of magnetic horn and neutrino beam. Proc. Int. Conf. on Instrumentation for High Energy Physics, 1962, Nucl. Instr. and Methods 20, 58 (1963)

9) B. de Raad, L. Resegotti - An experimental arrangement of the heavy liquid bubble chamber in the neutrino search, CERN - PS/Int. EA 60-16

10) B. Kuiper, D. Lake, G. Plass - Computation of trajectories in the C.P.S., CERN - PS/Int. EA 59-14

11) Measurements on the prototype magnet unit, CERN - PS/Int. MM 59-5

12) S. van der Meer - An improved beam optics programme, CERN-NPA/Int. 62-3

13) G.K. O'Neill, V. Korenmann - The delay-line inflector, Princeton Pennsylvania Accelerator Project GKON 10 - VK 13 (1957)

14) G.K. O'Neill - Storage rings for electrons and protons, Proc. Int. Conf. on High Energy Accelerators and Instrumentation, CERN, Geneva 1959

15) R.A. Fitch, N.R. McCornick - Low inductance switching using parallel spark gaps, J.E.E. Convention on Thermonuclear processes, 1959

16) R. Bertolotto et al. - The fast ejection system of the CERN 25 GeV proton synchrotron, CERN-NPA/Int. 63-15 or Proc. Int. Conf. on High Energy Accelerators, Dubna 1963

17) D.A.G. Neet - Accurate current supplies and electronic controls for the pulsed magnets of the neutrino beam CERN-NPA/Int. 62-9

18) B. Langeseth - A pulsed beam transport system, CERN-NPA/Int. 63-19

19) B. de Raad - Setting-up of the enhanced neutrino beam, CERN-NPA/Int. 61-28

20) Ch. Brooks - An induction type monitor for the fast ejected beam, MPS/Int. VA 63-6.

21) D.A.G. Neet - Proposed electronic controls for the South Hall fast ejection system, CERN-NPA/Int. 61-19.

Table 2

Parameters of kicker magnet circuit (per unit)

Number of units		2	
Gap height	Ferrite	22	mm
	useful for beam	15	mm
Gap width	Ferrite	32	mm
	useful for beam	25	mm
Length		450	mm
Ferrite length		280	mm

Pulse duration	2.1 μs		0.10 μs *
Delay time kicker	~ 0.07	μs	
Inductance of kicker	~ 0.7	μH	
Capacitance of kicker	~ 6600	pF	
Characteristic impedance	~10.4	Ω	
Max. kicker voltage **	35	kV	
" line voltage	70	kV	
" current	3500	A	
" energy in storage line	260 J		13 J *
" magnetic energy in kicker	9.3	J	
" electrostatic energy in kicker	9.3	J	
" obtainable kick in entire magnet	0.153	Wb/m	
" field in Ferrite	~ 0.3	Wb/m^2	

* value for single bunch ejection

** maximum means highest value used over at least 10^6 operations

Table 3

Parameters of the bending magnet circuit

Magnet aperture	45	mm wide
	25	mm high
Magnetic length	1.96	m
Inductance of the magnet	4.2	μH
Onset of saturation effects	around 1.5	Wb/m^2
Current at 1.5 Wb/m^2	30	kAmp
Pulser capacitor (HYDRA)	328	μF
Capacitor voltage at 1.5 Wb/m^2	4.5	kV
Crowbar resistor	0.1	Ω
Crowbar circuit inductance	0.2	μH
Ringing frequency	3.5	kHz
Crowbar delay	110	μs

Table 4

Parameters of the beam transport magnets and the pulser circuits

Max. ratings and values for the present beam at 25 GeV/c

	Quadrupole lenses				Horizontal deflecting magnets	Vertical correction magnet	Unit
	Q 1	Q 2	Q 3	Q 4			
Magnetic length	0.455	0.455	1.485	1.485	1.10	0.35	m
Magnetic aperture	40 dia.	40 dia.	40 dia.	40 dia.	66 x 40	40 x 66	mm, mm^2
Magnetic flux density, max.	---	---	---	---	2.2	2.2	Wb/m^2
Magnetic flux density at 25 GeV/c	---	---	---	---	1.56	0.03	Wb/m^2
Magnetic field gradient, max.	80	80	80	80	---	---	Wb/m^2
Magnetic field gradient at 25 GeV/c	26	42	36	41	---	---	Wb/m^2
Excitation current	0.85	1.35	1.15	1.30	1.65	0.03	kA
Inductance	0.4	0.4	1.2	1.2	3.2	1	mH
Pulser capacitor	278	556	1390	1663	3892	10	μF
Capacitor voltage	1.1	1.3	1.3	1.3	1.7	1.0	kV
Stored energy	0.17	0.47	1.18	1.42	5.65	0.010	kJ
Oscillation frequency	440	330	120	110	45	1600	c/s

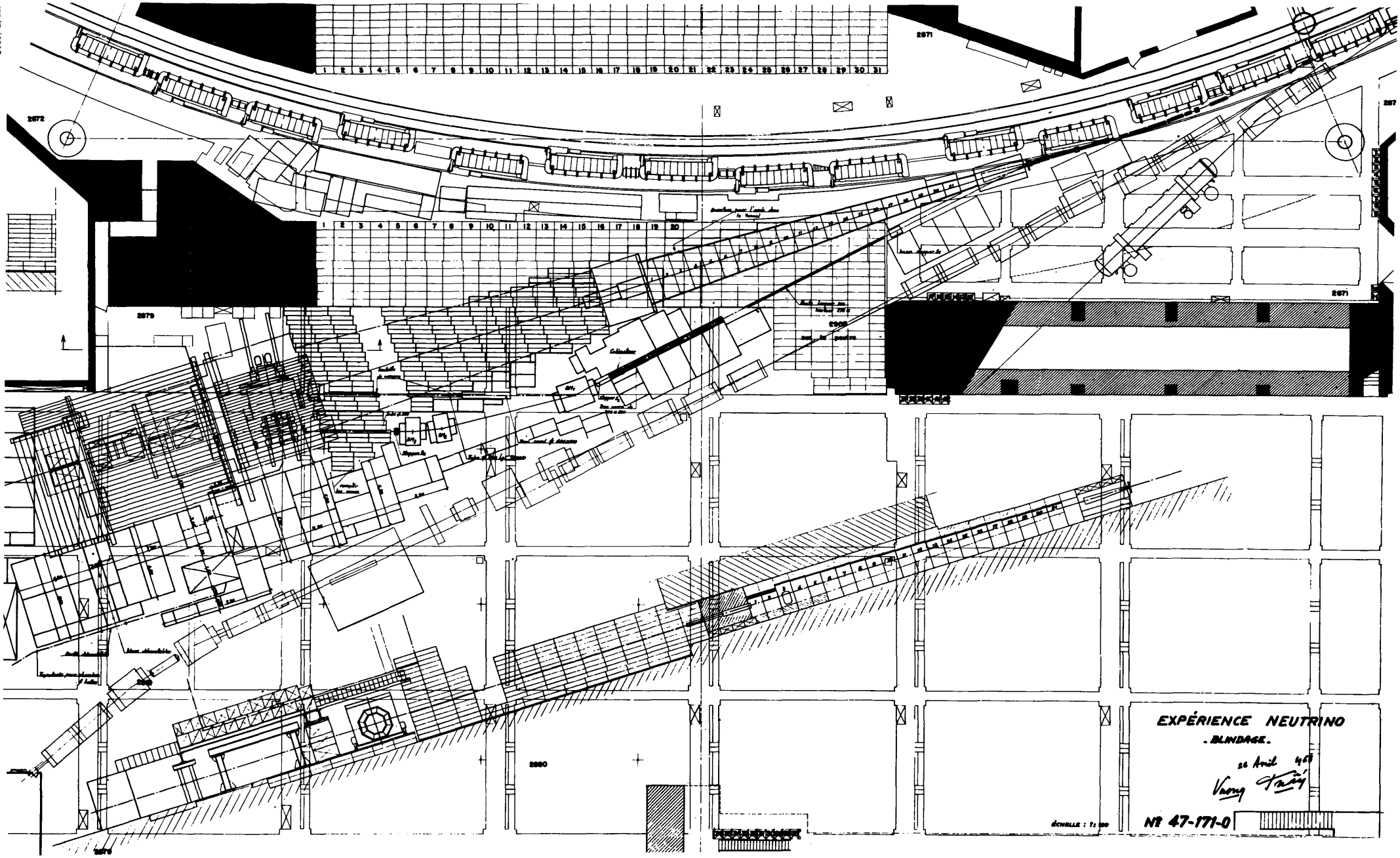
EXPÉRIENCE NEUTRINO
. BLINDAGE .
26 Avril 49
Vu et Approuvé
N° 47-171-0
2871
2872
2879
2880

Fig. 1

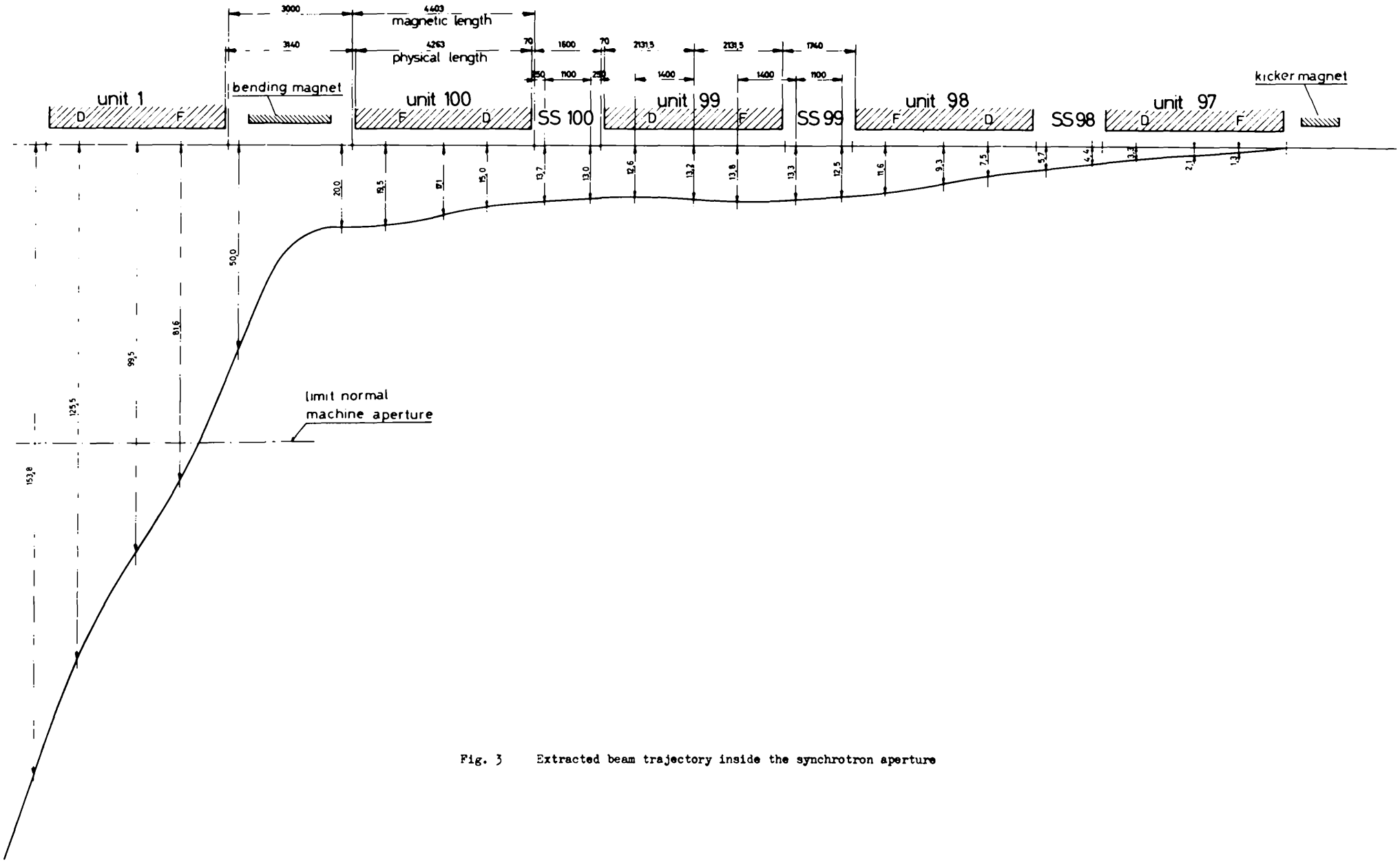

Fig. 3 Extracted beam trajectory inside the synchrotron aperture

SIS/H/6619

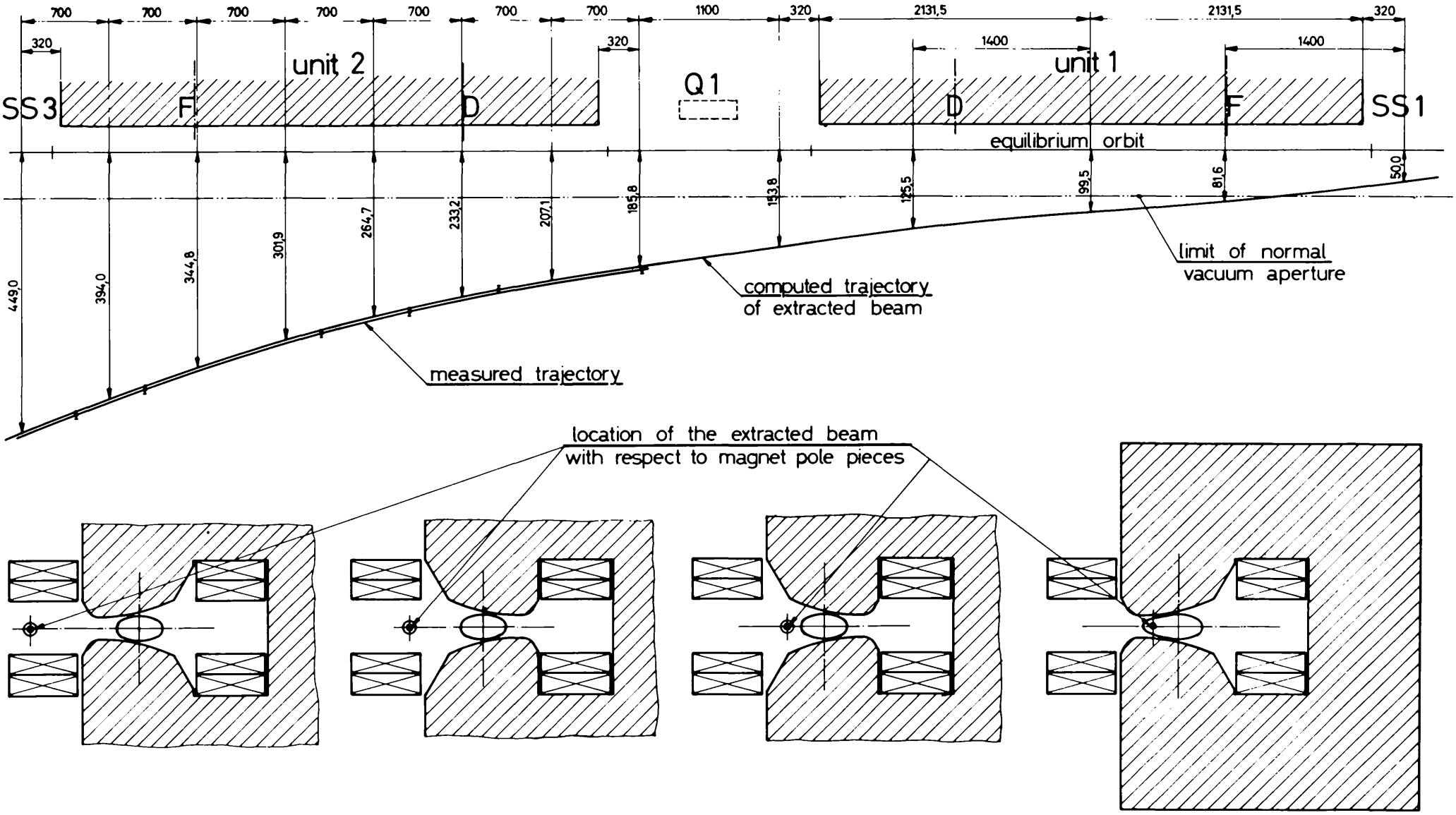

Fig. 4 Extracted beam trajectory in the synchrotron leakage field

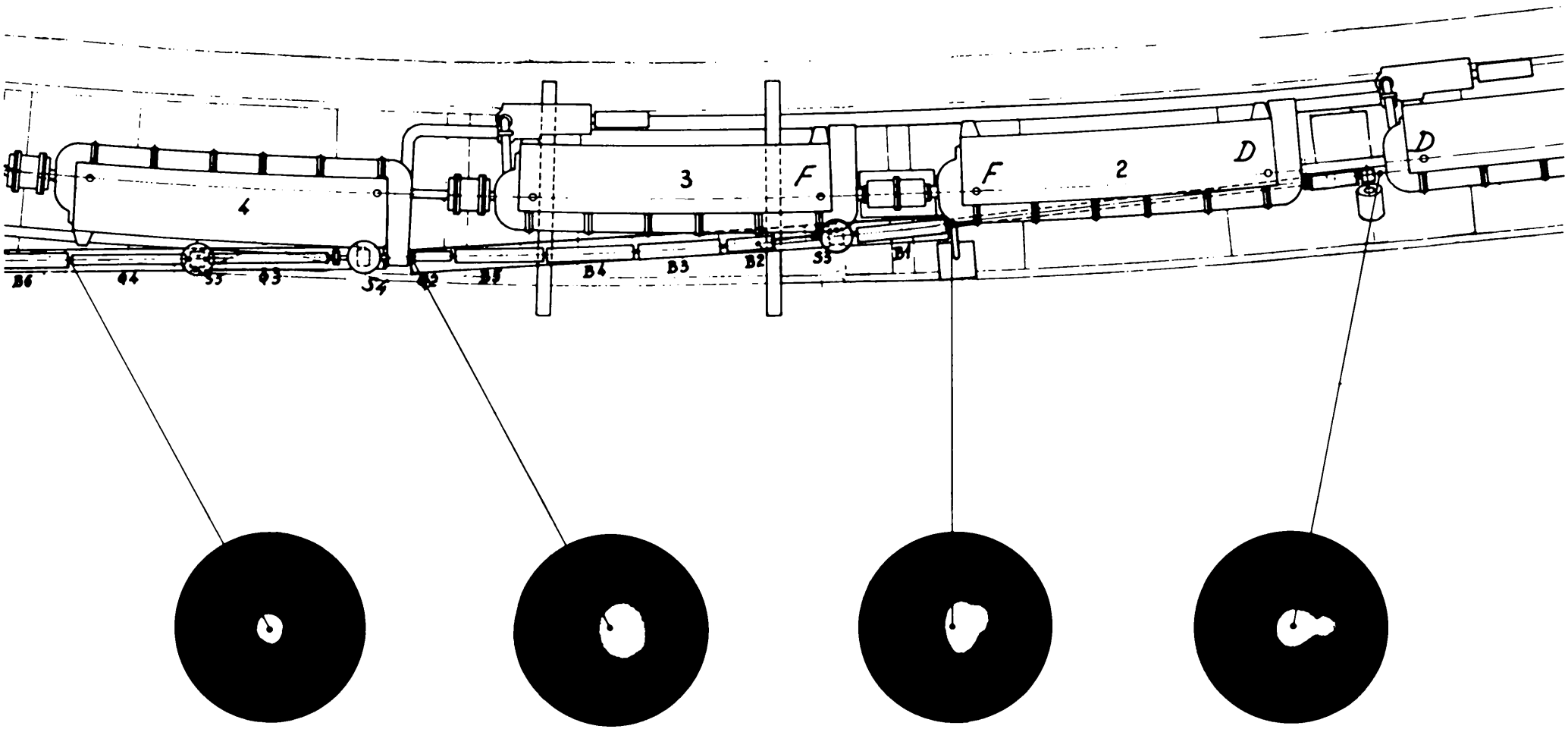

Fig. 5 Cross section of the extracted beam along the external beam path

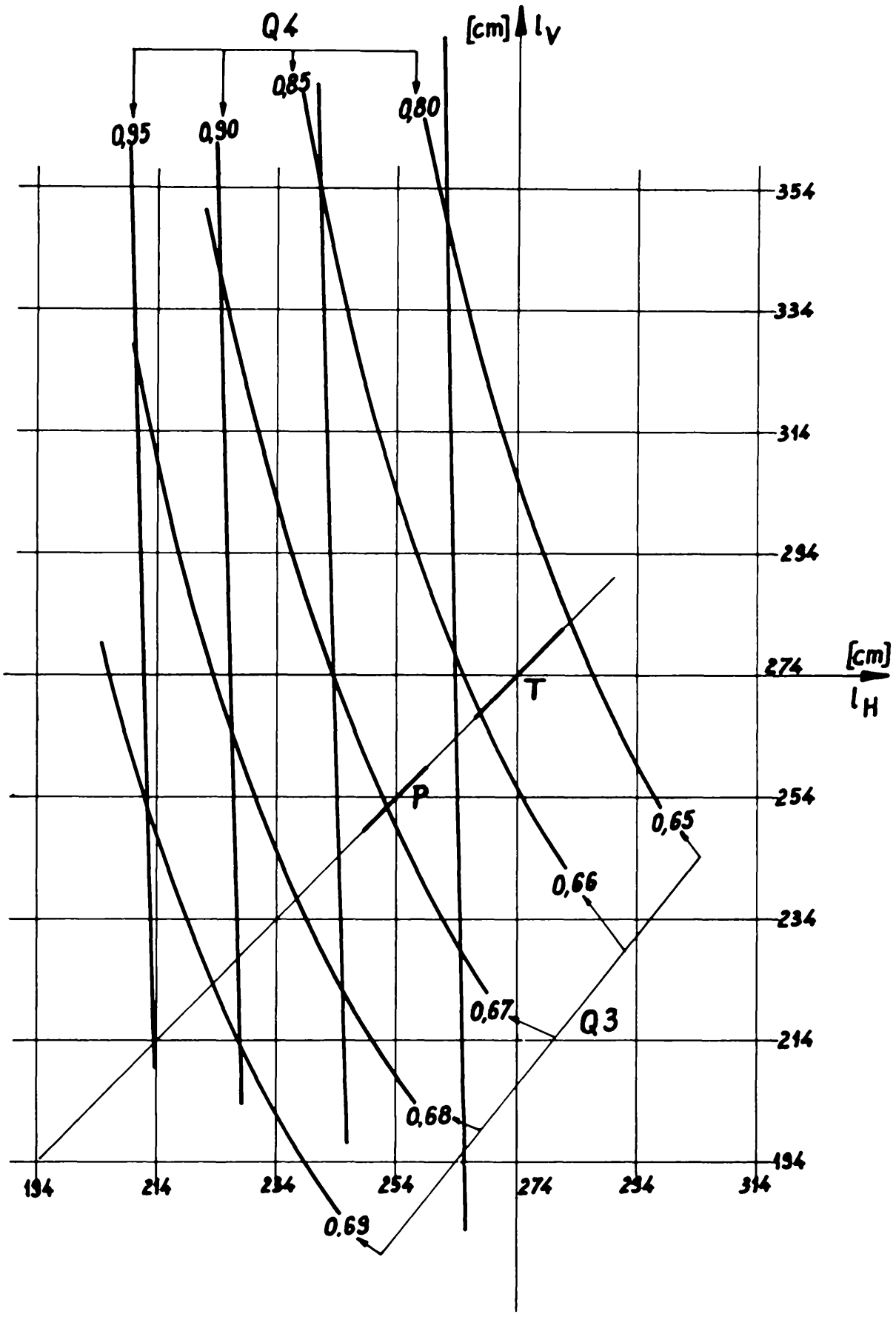

Fig. 6 Dependence on the strengths of Q 3 and Q 4 of the distance of the cross-over points from the centre of the last quadrupole (Q 4) for horizontal and vertical planes

strength of Q 1 : 0.15 m^{-1}

strength of Q 2 : 0.24 m^{-1}

T : location of the target

P : place of focus for tests

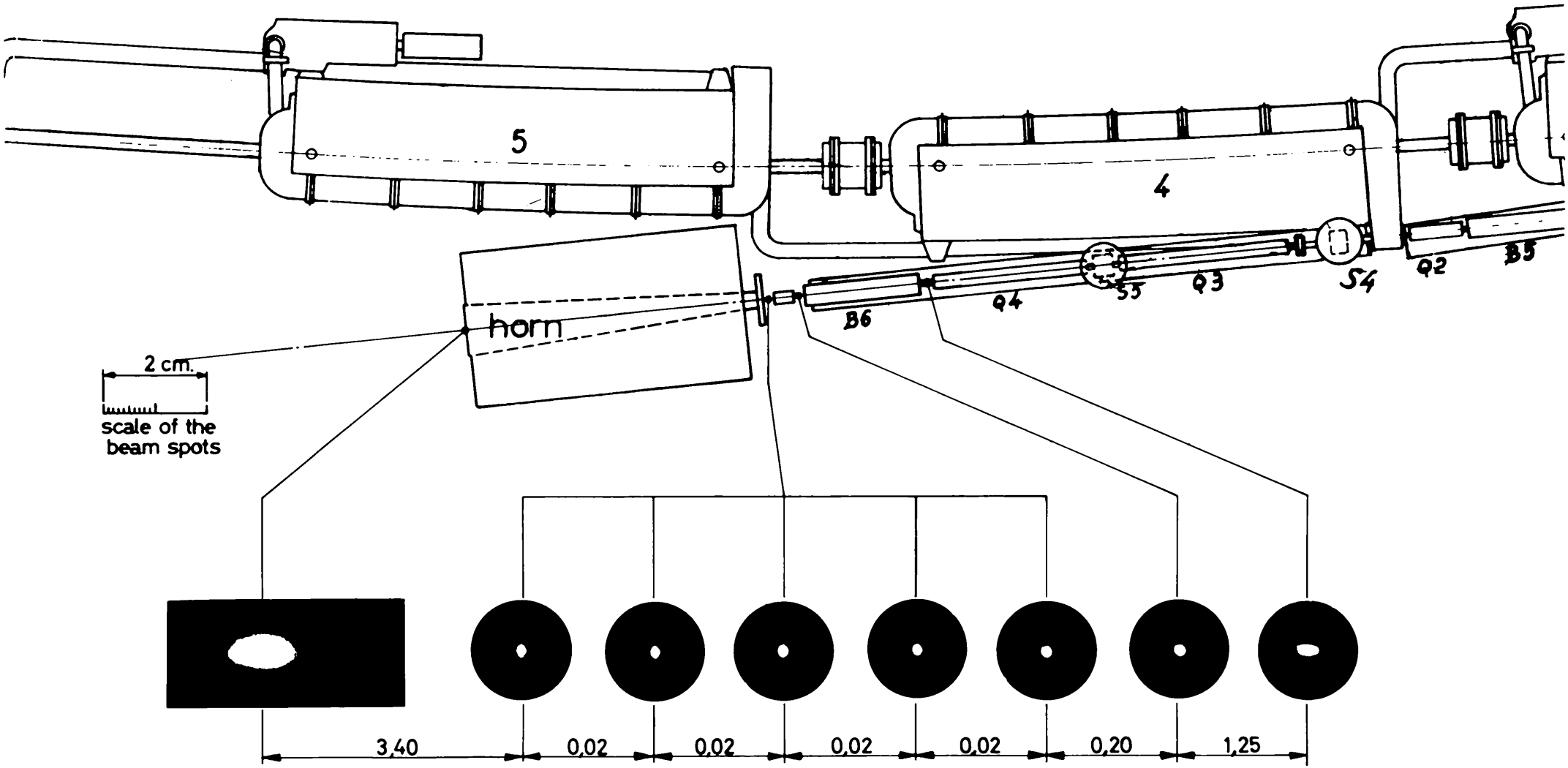

Fig. 7 Beam cross sections in the vicinity of the target. (Lenses tuned to produce focus in the space in front of the horn, cp. fig. 6).

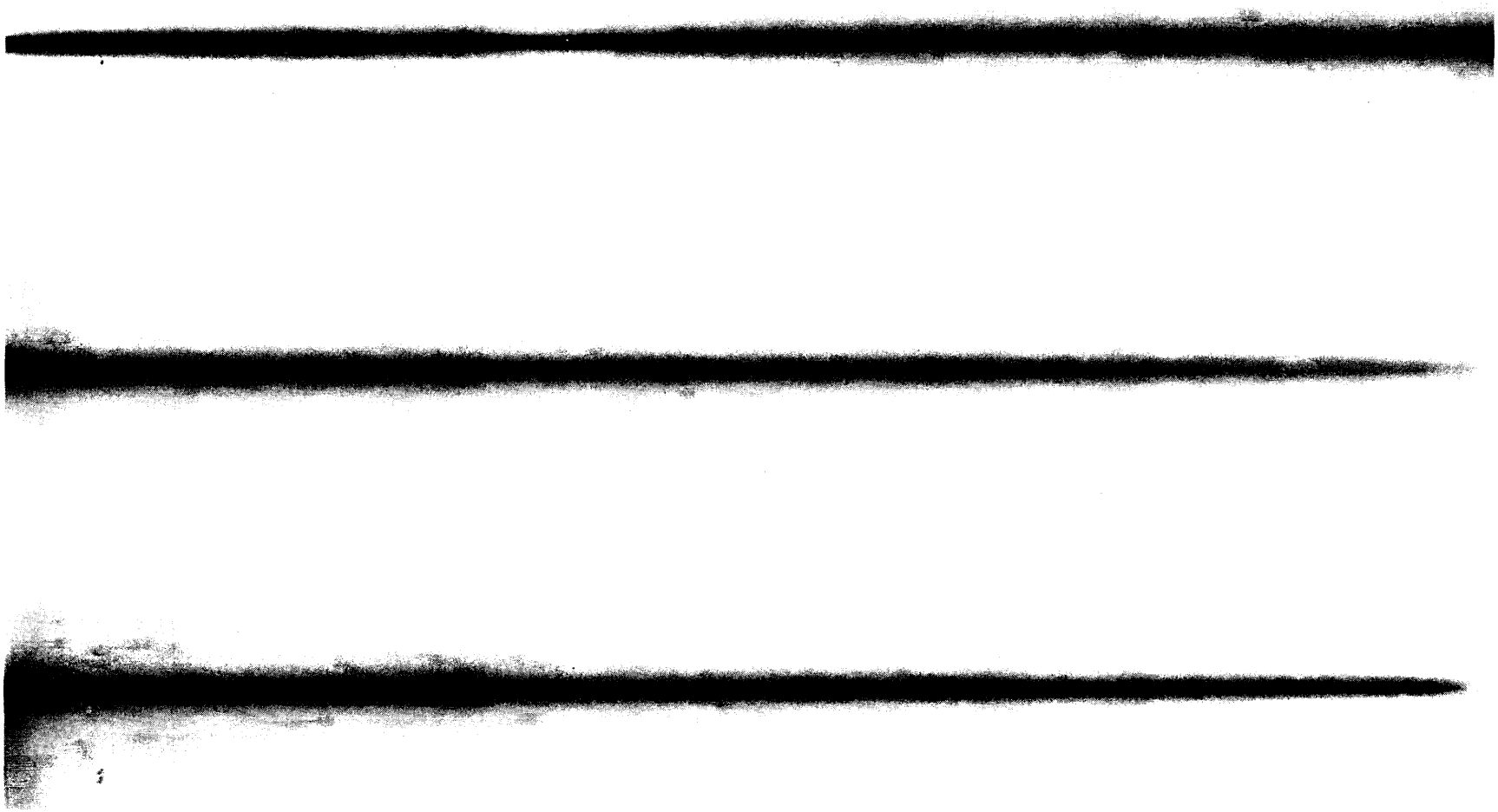

Fig. 8 Longitudinal sections of the beam in front of the target. Top : vertical section, below : two horizontal sections (not well aligned with the beam axis).

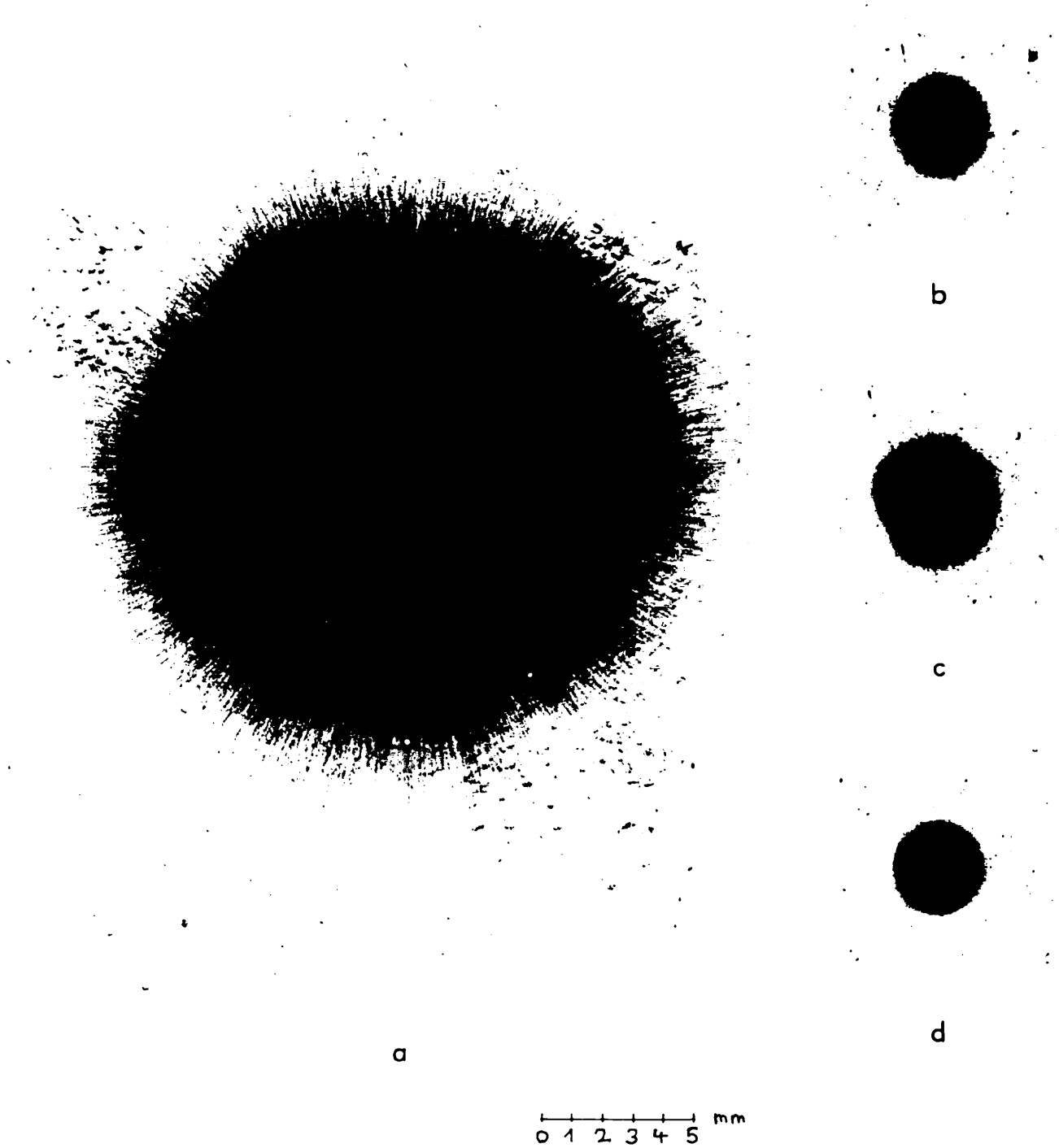

Fig. 9 Images obtained on (a) G 5 and (b,c,d) K - 1 emulsions by exposing to doses of 1.6 x 10^{10} protons. (Enlargement ~ 5 x). a) and c) obtained from one pulse of 20 bunches, b) from one single bunch and d) from 20 single bunches of subsequent machine pulses.

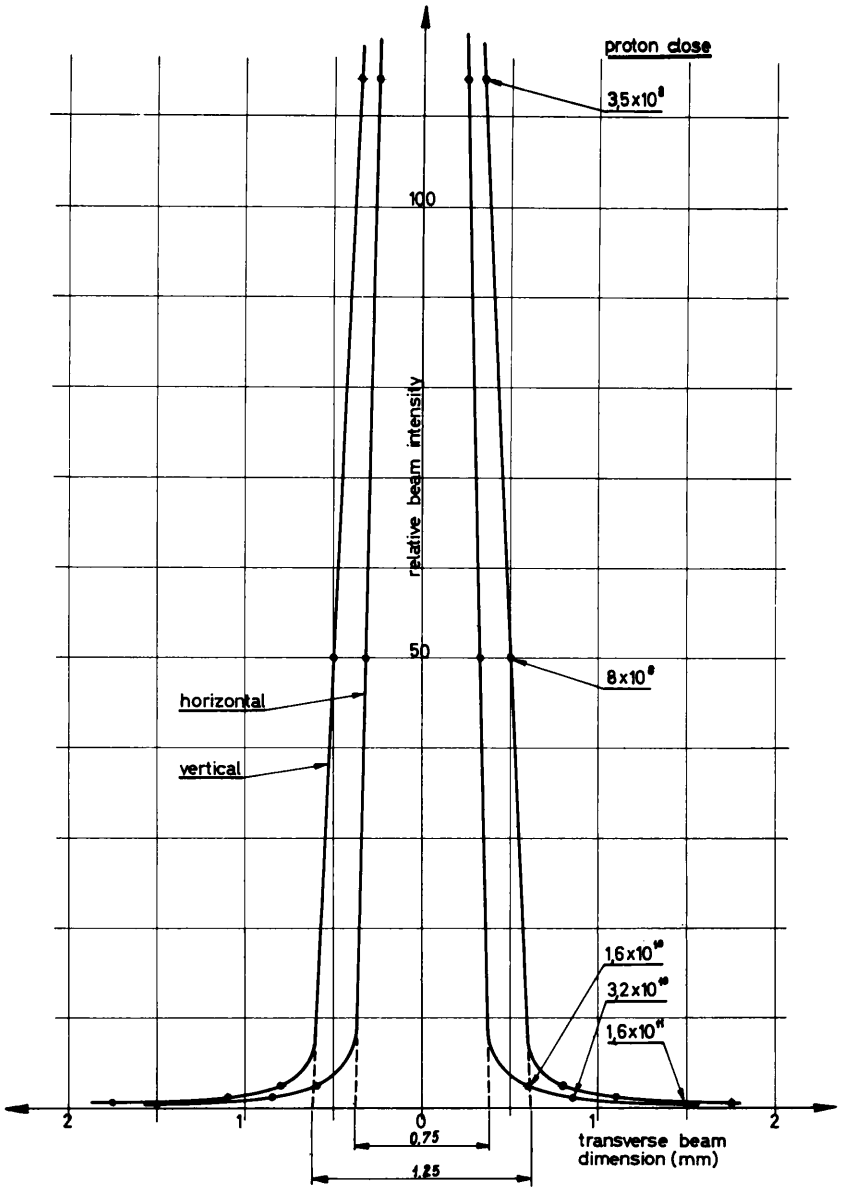

Fig. 10 Intensity distribution at the edge of the extracted beam, as obtained from the exposure of K - 1 emulsions to the indicated doses

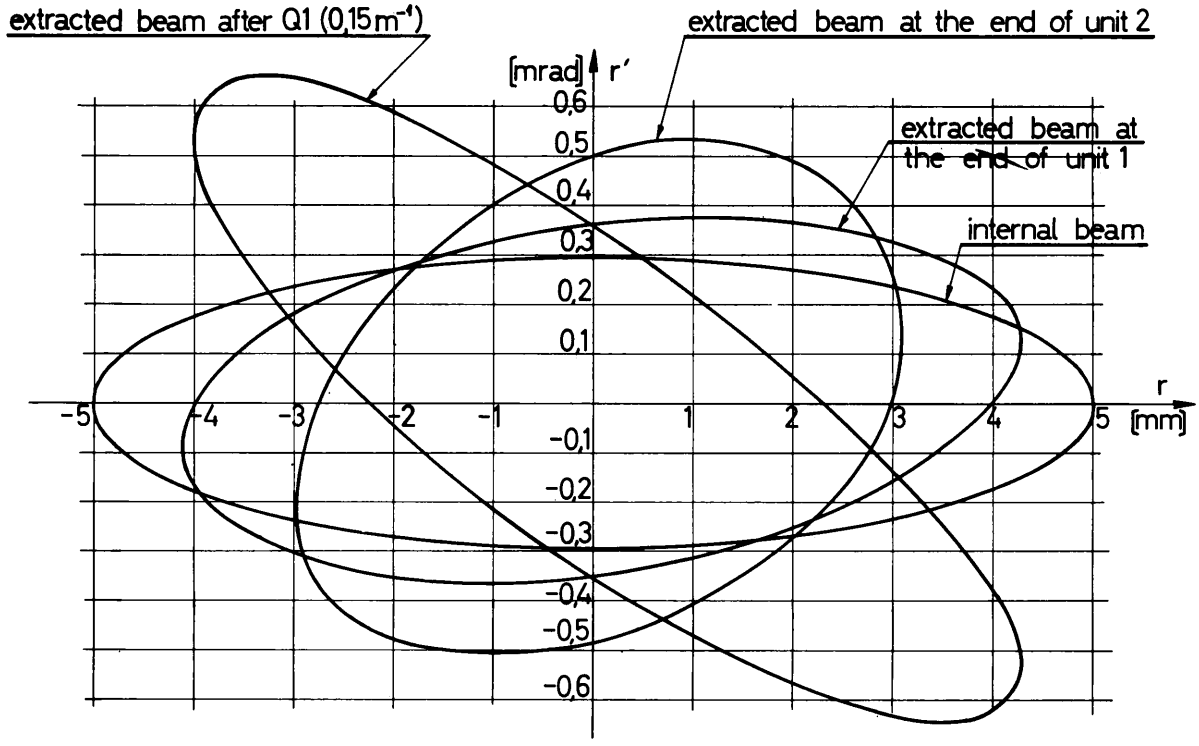

Fig. 11 Computed horizontal phase - space contours for beam traversing the P.S. leakage field.

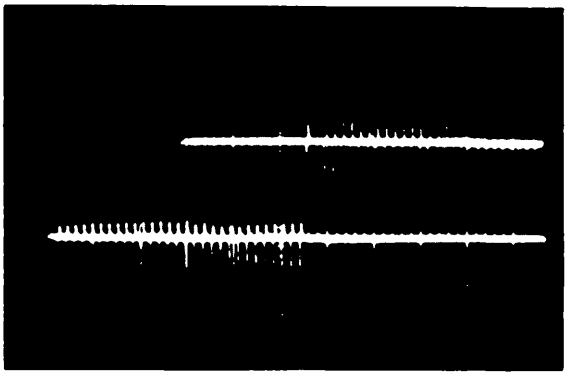

Fig. 12 Time structure of the beam. Bottom trace : circulating beam, top trace : ejected beam.

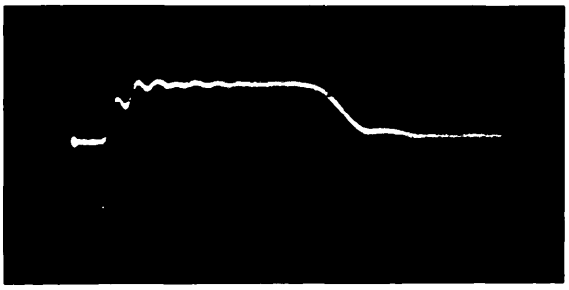

Fig. 13 Sum of magnetic kicks in the two kicker magnet units. Each derived from a loop through the entire length of the unit. Sweep: 0.5 μs/div.

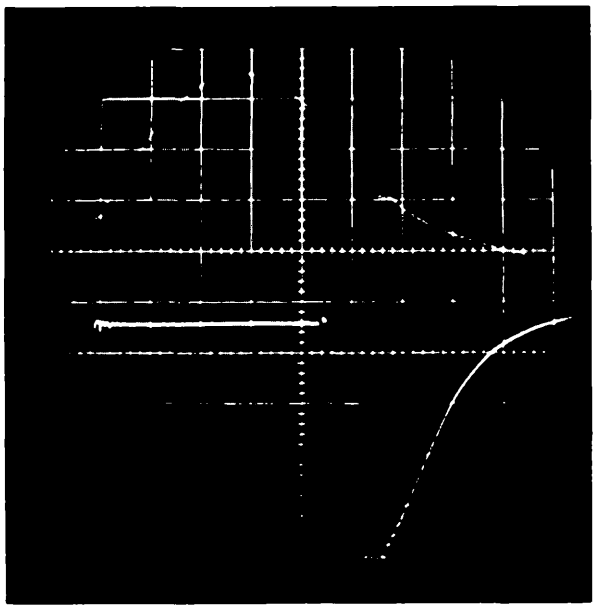

Fig. 14. Top: Bending magnet current. Bottom: Crowbar current.

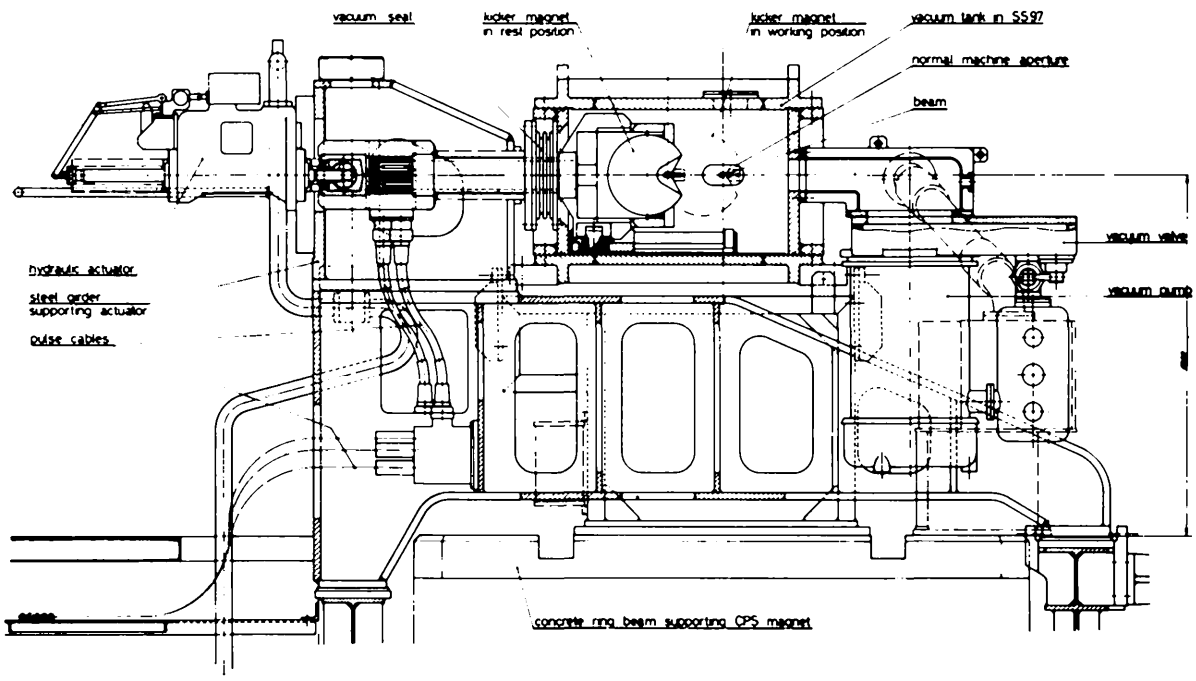

Fig. 15 a. Sectional view of the kicker magnet in its vacuum tank.

b. Kicker magnet, being aligned in its tank.

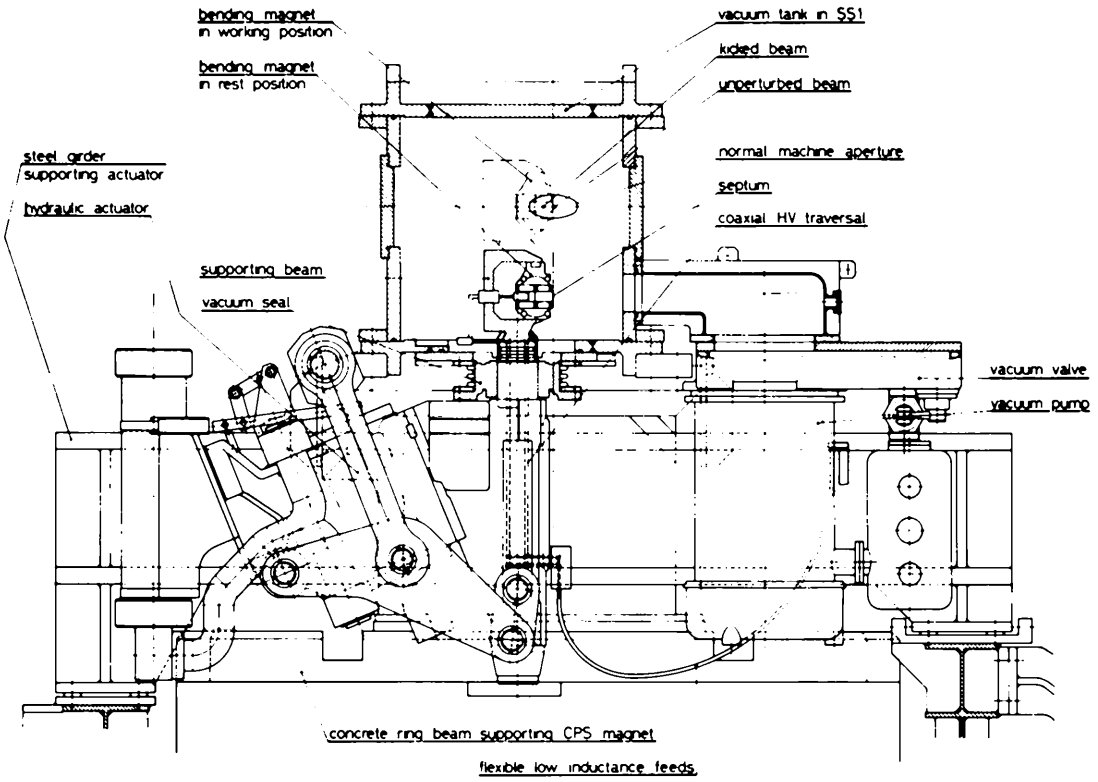

Fig. 16 a. Sectional view of the bending magnet in its vacuum tank.

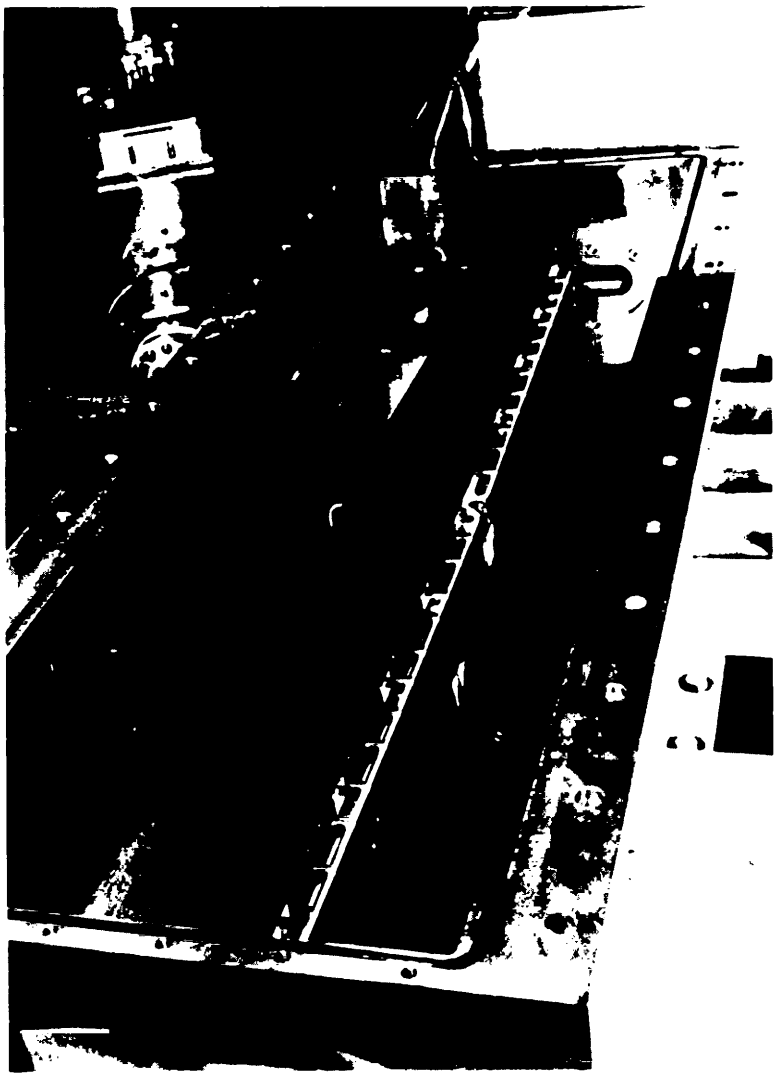

b. Bending magnet in its working position.

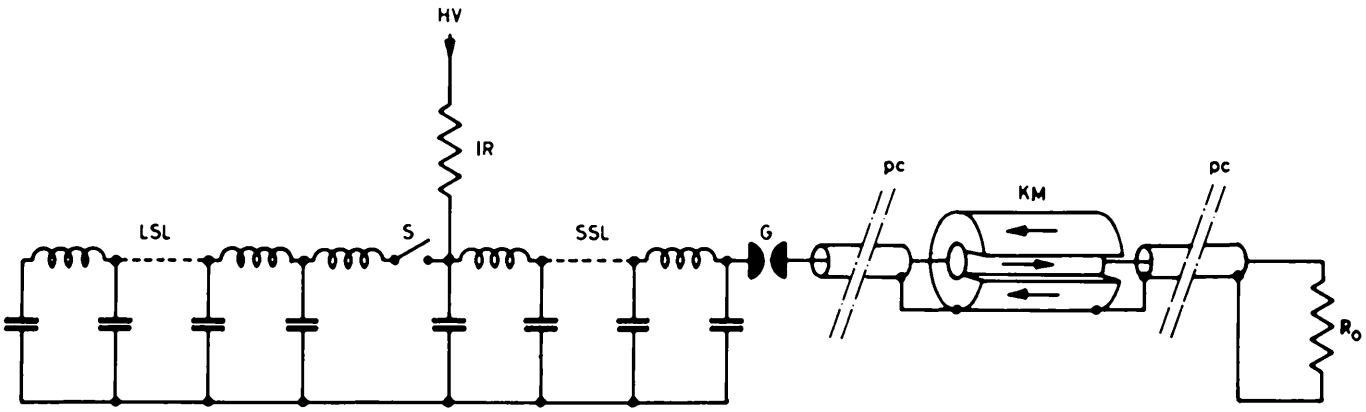

Fig. 17 Principle of the kicker magnet circuit. HV = charging line from high voltage set ; IR = isolating resistor ; LSL = long storage line ; S = switch (when closed: 2 μs pulse; when open: 100 ns pulse); SSL = short storage line; G = sparkgap; pc = pulse cables; KM = kicker magnet; R = matched terminating resistors.

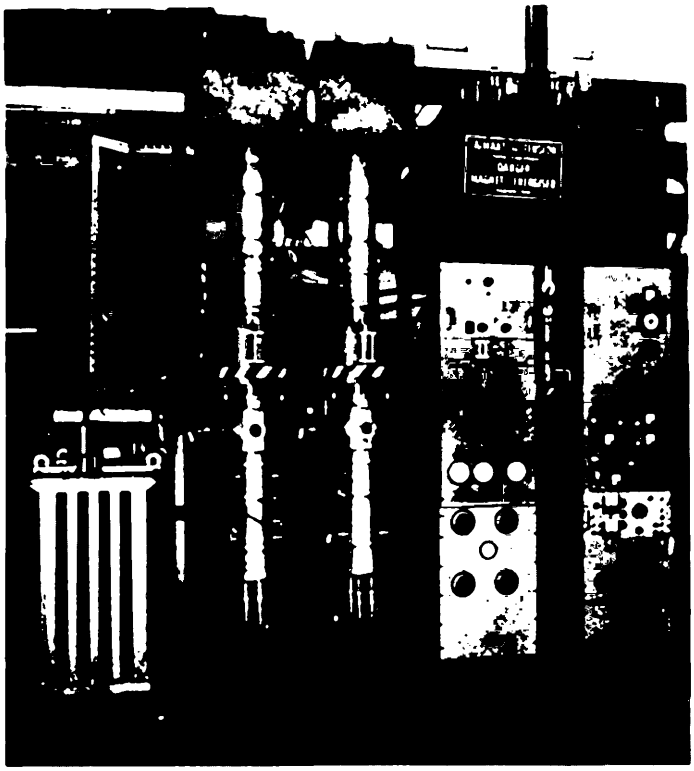

Fig. 18 Pulse generators for the kicker magnet. Center: Two coaxial lines with sparkgaps. Left: High voltage set. Right top: High voltage distribution box. Lower right side: Triggering gear and local controls.

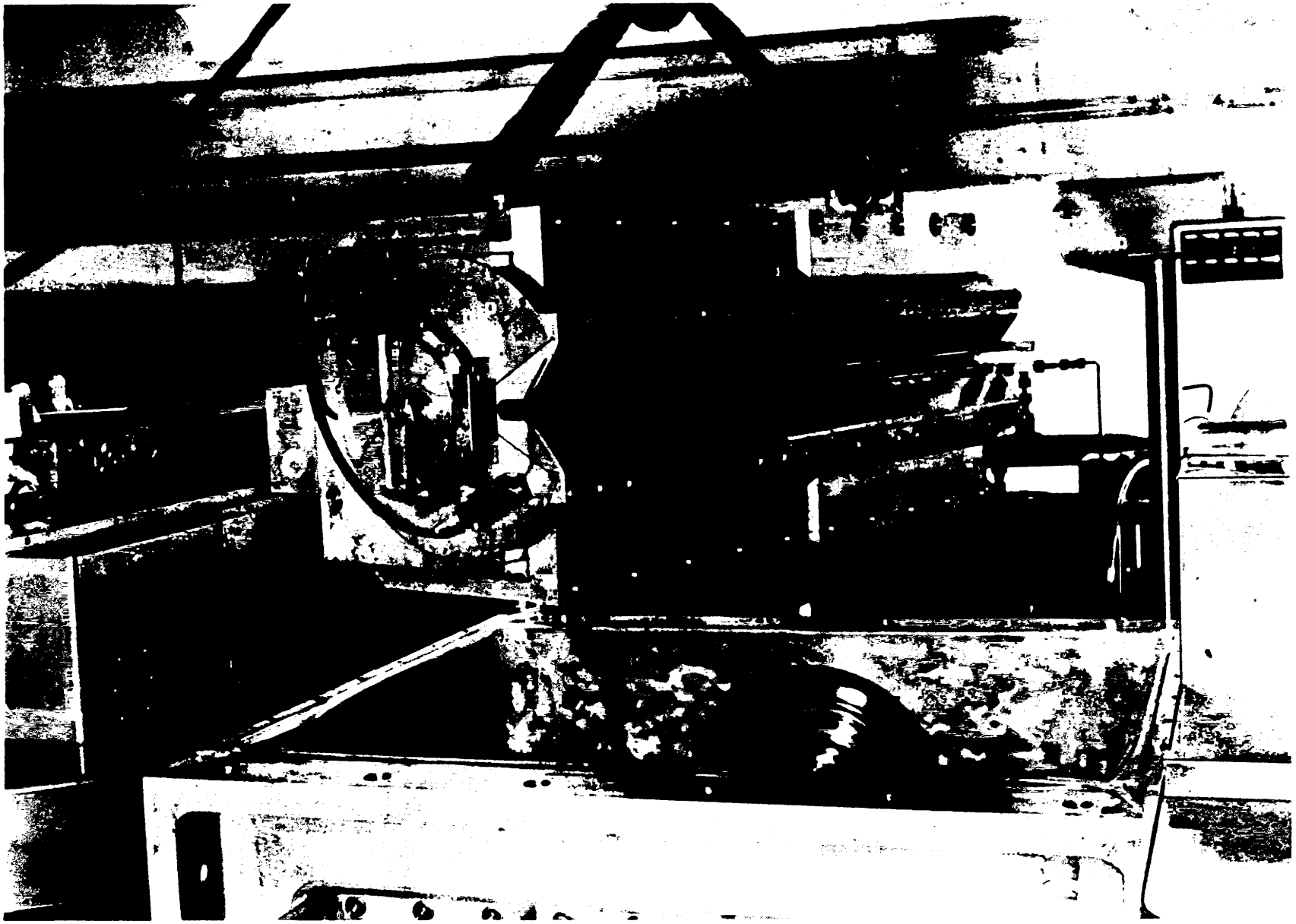

Fig. 19 Assembled kicker magnet above its vacuum tank. Front left: Cable coming from the pulse observation loop in the gap. On the other end of the magnet: The beam-razor fork.

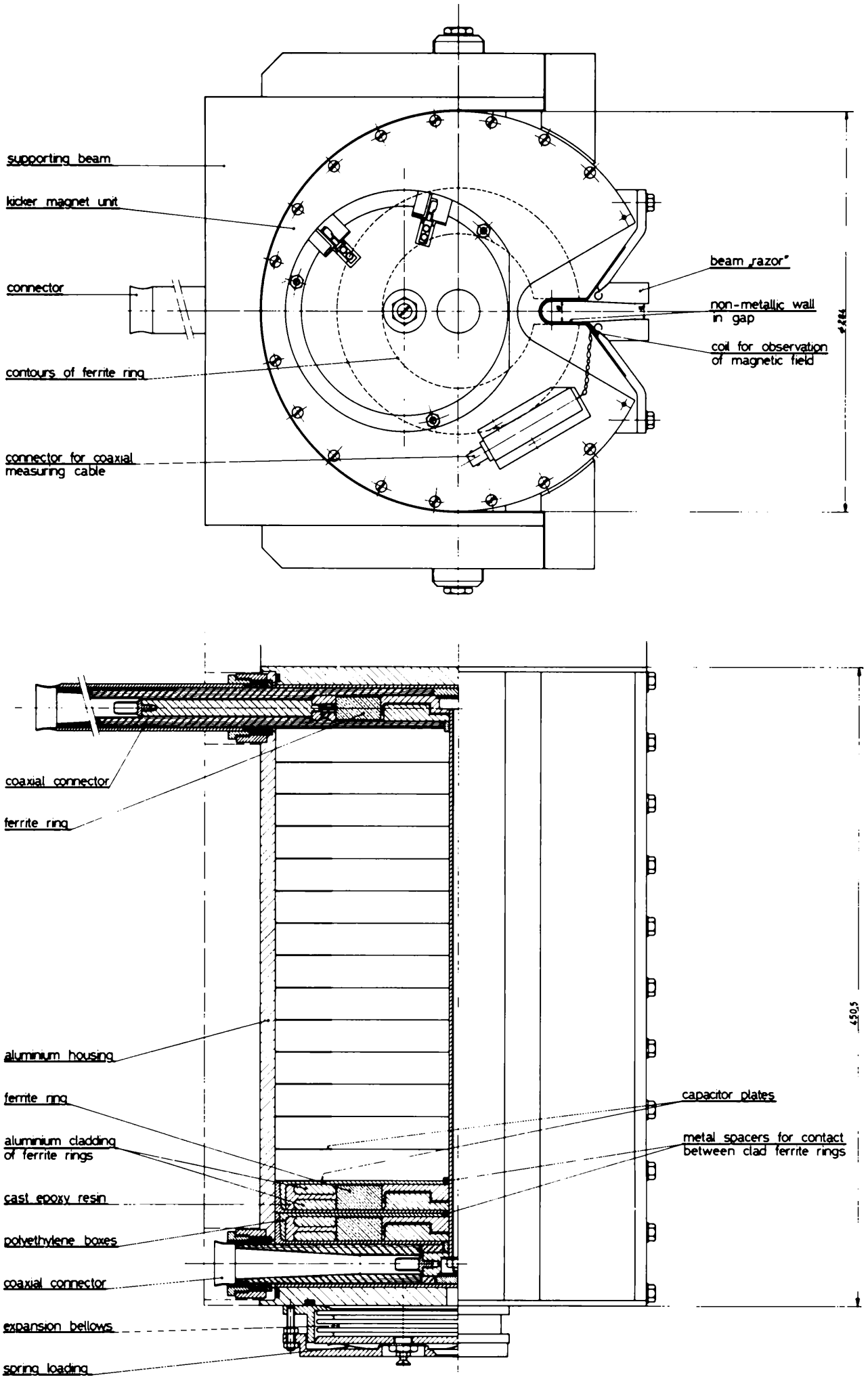

Fig. 20 Structure of the kicker magnet. Top: View on one end of the assembled magnet. Bottom: Horizontal section of one unit.

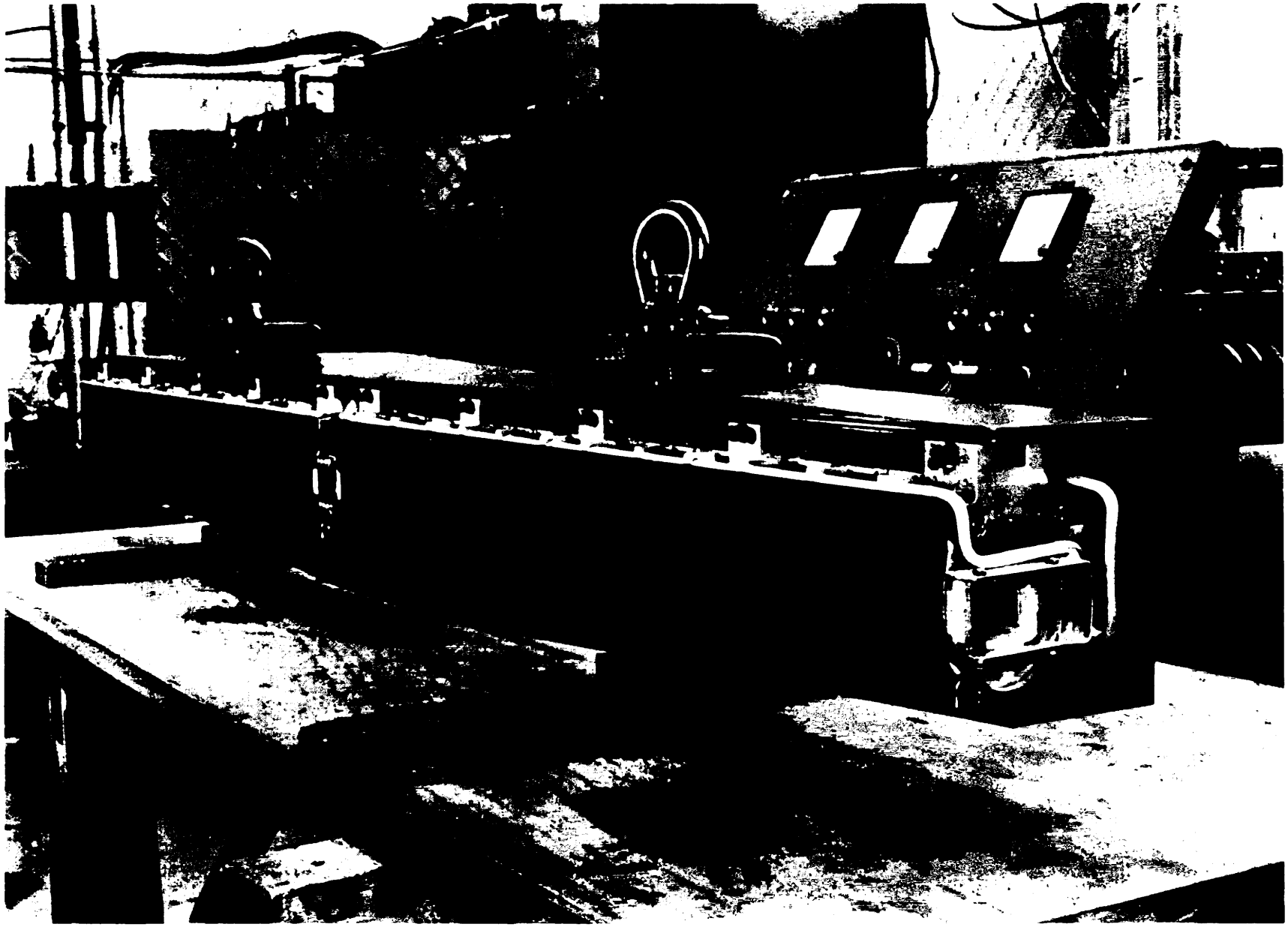

Fig. 22 Assembled bending magnet. Black plate in front is the eddy current shield for reducing the leakage field.

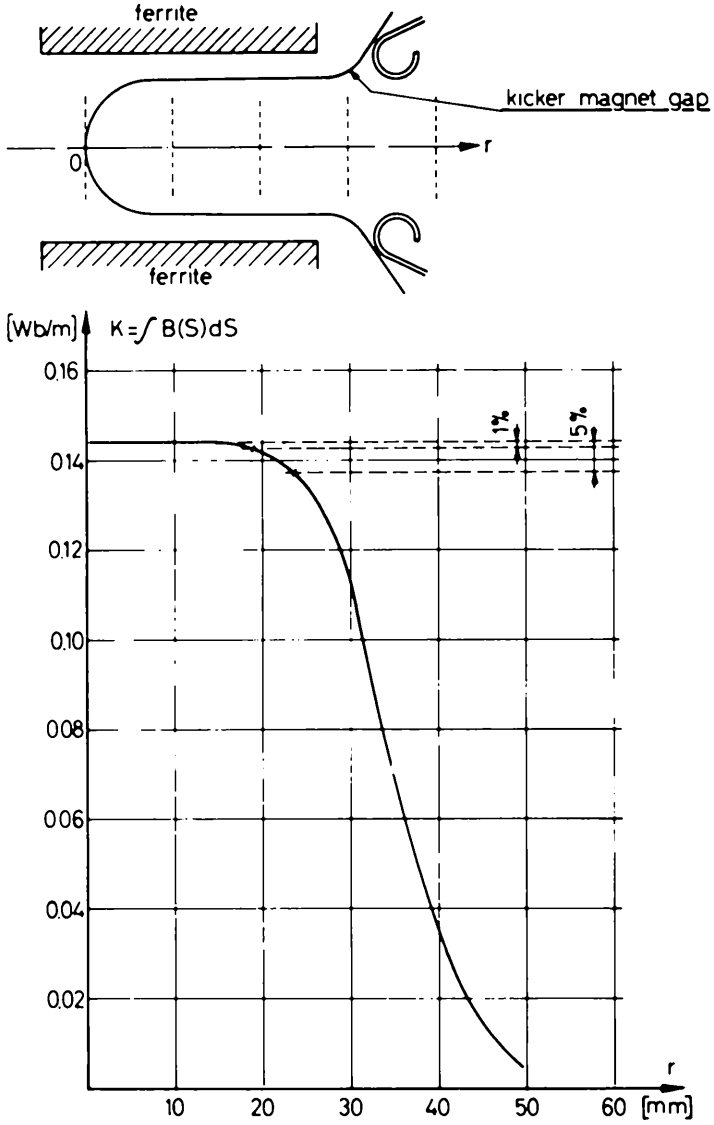

Fig. 21 The kick K as a function of the radial position in the gap of the kicker magnet.

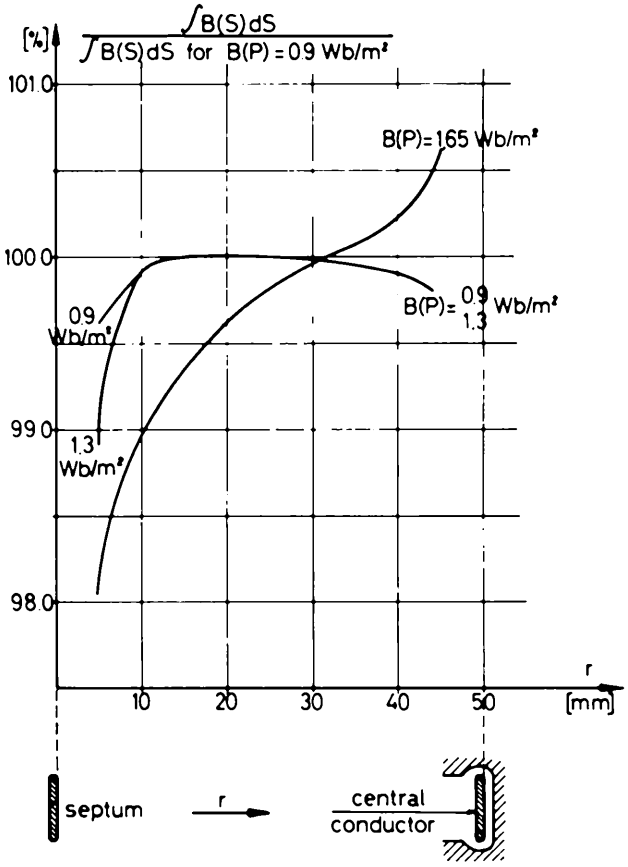

Fig. 23 Integrated field along the bending magnet as a function of the radial position in its gap. Expressed as a percentage of its value at r = 20 and at a field B (P) = 0.9 Wb/m² in the reference point P (cp. sketch of fig. 20).

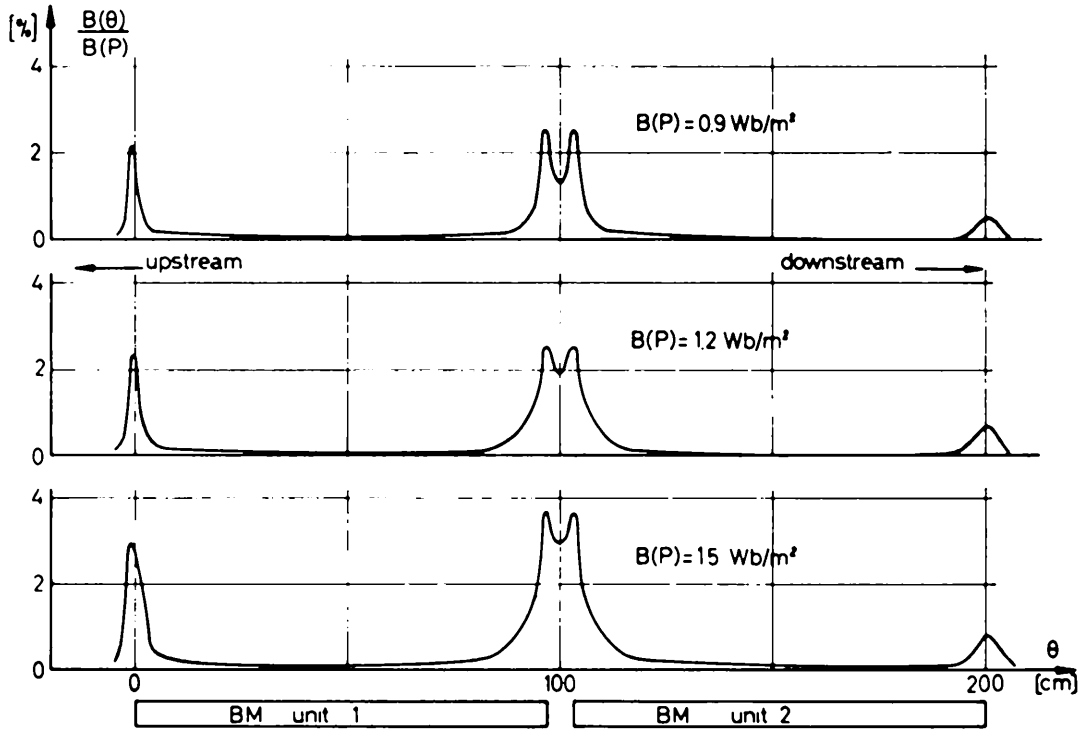

Fig. 24 Leakage field of the bending magnet as measured point to point along the undisturbed machine orbit (cp. the sketch of fig. 20). Expressed as a percentage of the field B(P) in the reference point P.

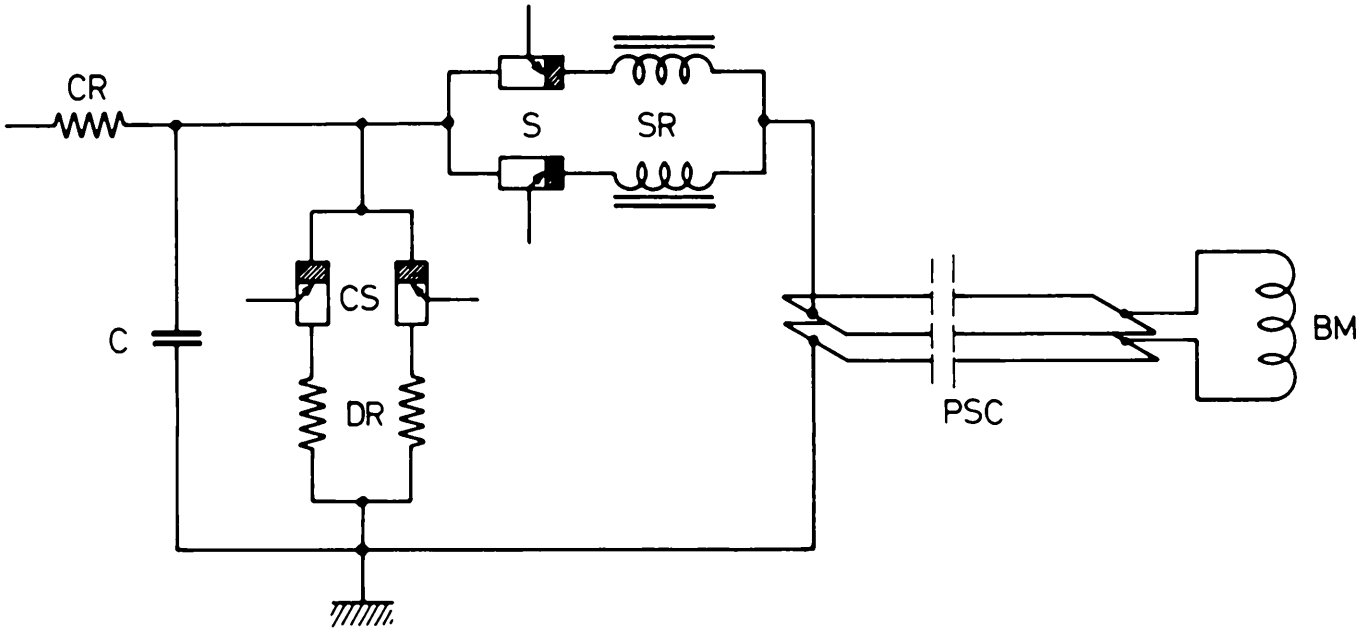

Fig. 25 Principle of bending magnet circuit. CR = charging resistor; C = capacitor bank; S = switching ignitrons; SR = saturable reactors; CS = crowbar switch; DR = dumping resistors; PSC = parallel strip conductors; BM = bending magnet.

Fig. 26 a

Bending magnet pulse generator. Front left: Ignitron rack. Behind that: Capacitor bank. Right: Ignitron and bending magnet temperature control.

Fig. 26 b

Ignitron rack. Top: Dumping resistor. Right: Ignitrons. Bottom: Saturable reactors. Center left: Low inductance shunts for current observation.

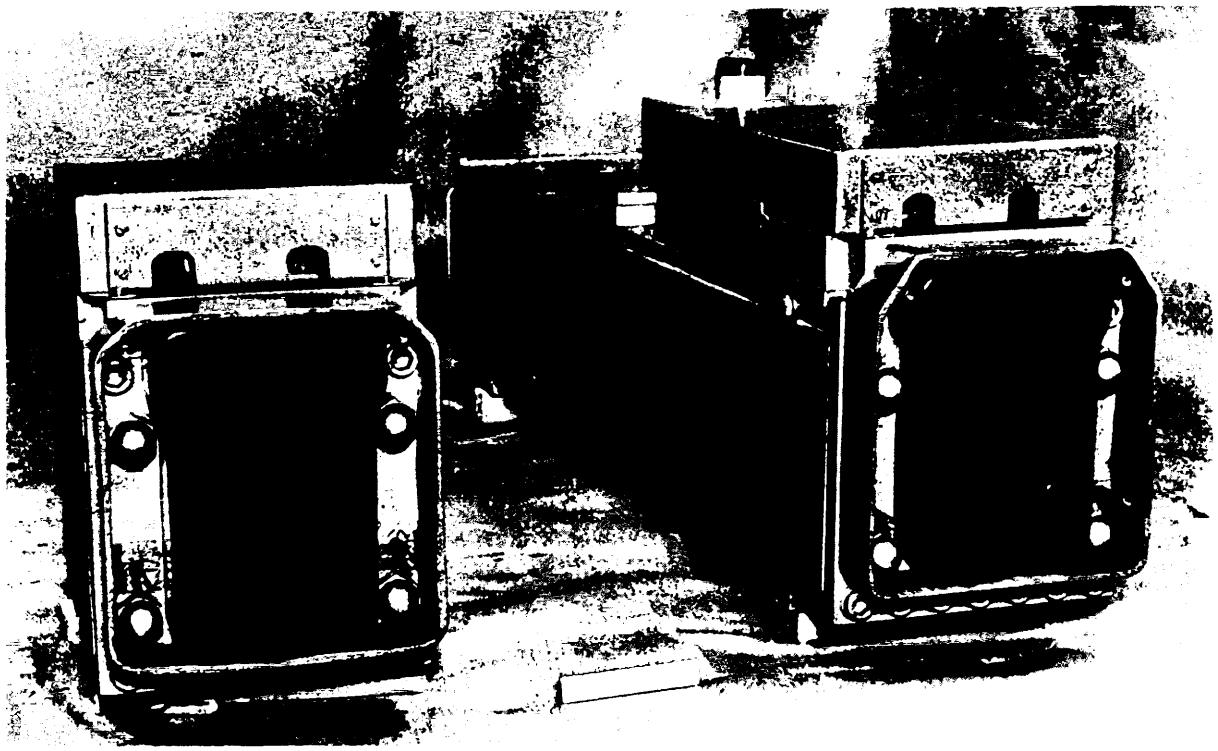

Fig. 27 Deflection magnets of the pulsed beam transport system

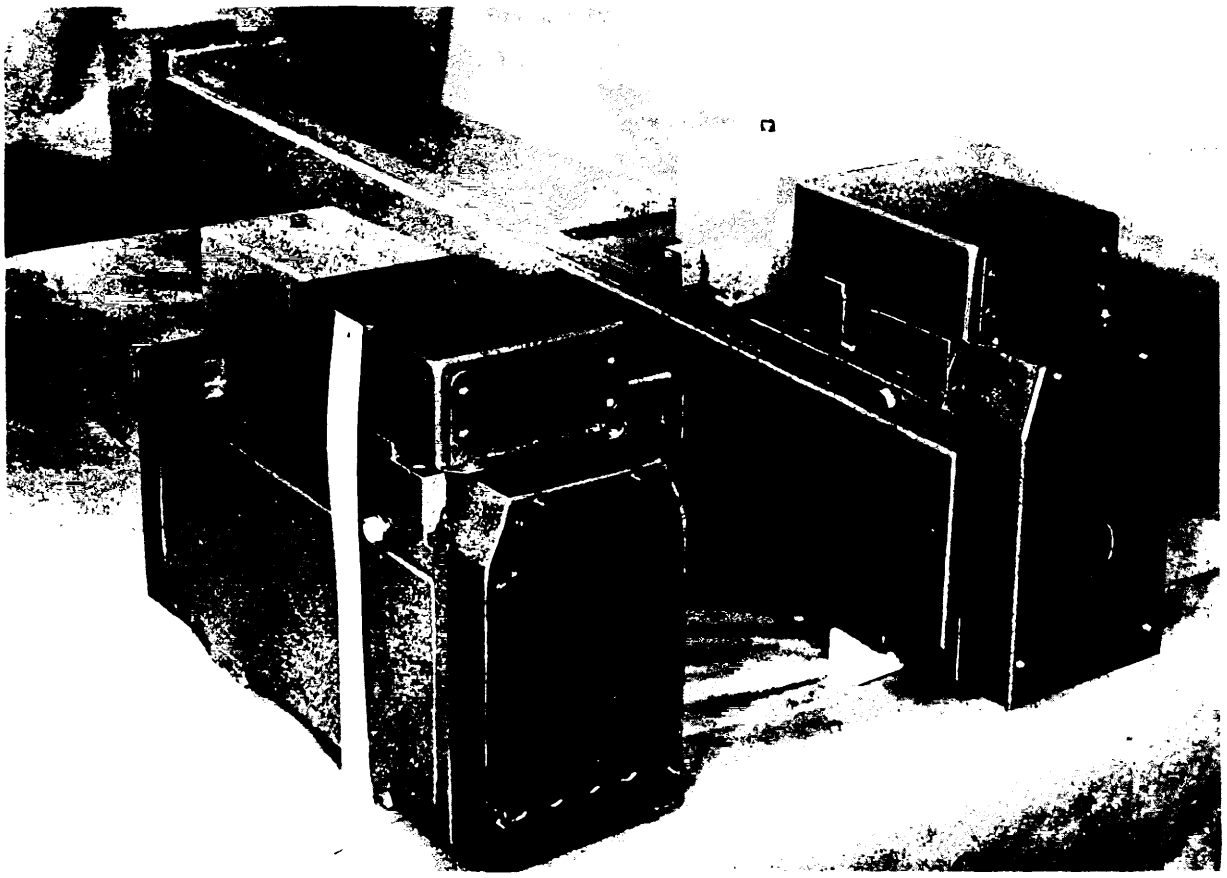

Fig. 28 Quadrupole lenses of the pulsed beam transport system

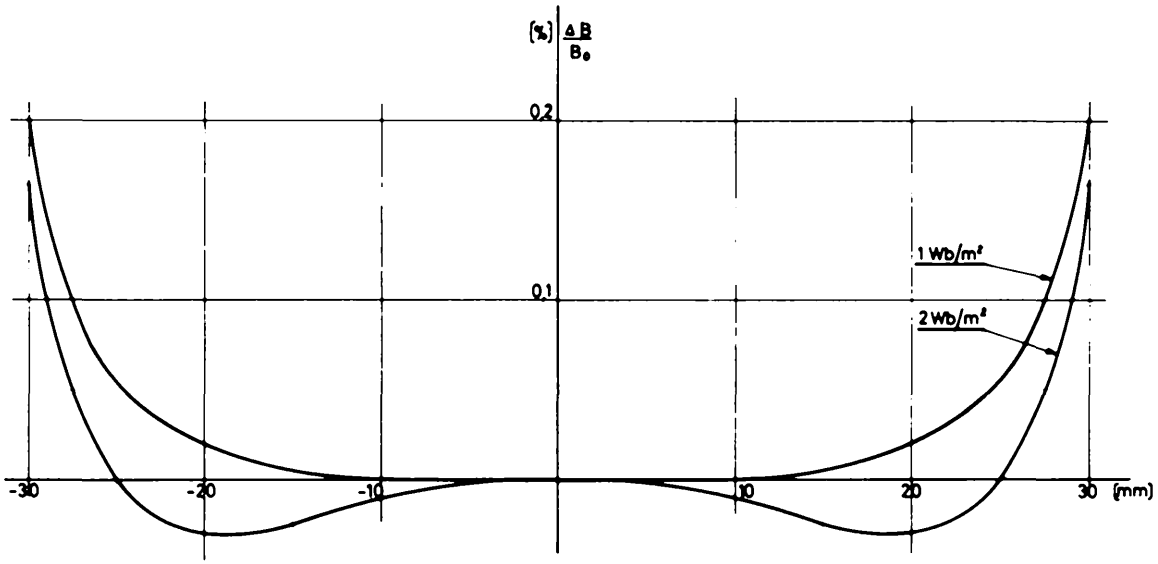

Fig. 29 Field error as function of transverse distance from axis of deflecting magnet

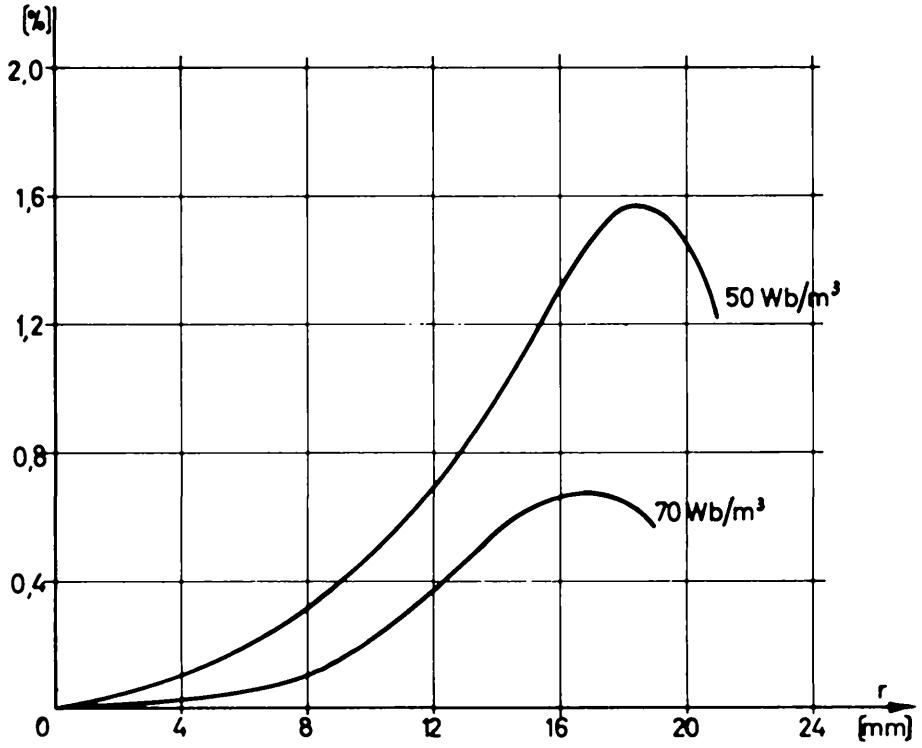

Fig. 30 Gradient error as a function of transverse distance from axis of quadrupole lens

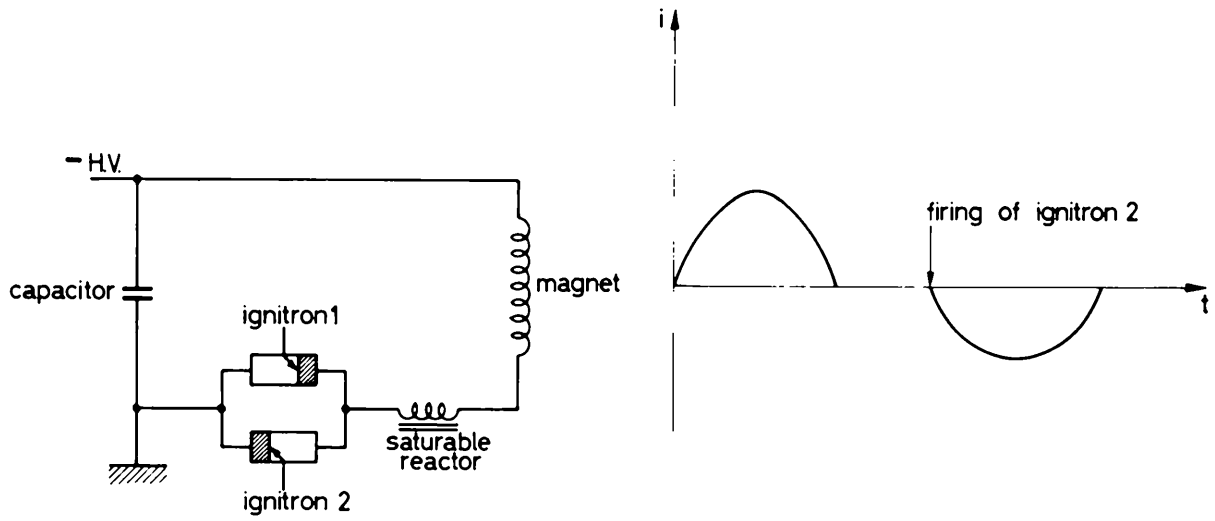

Fig. 31 Pulser circuit for pulsed beam transport magnets

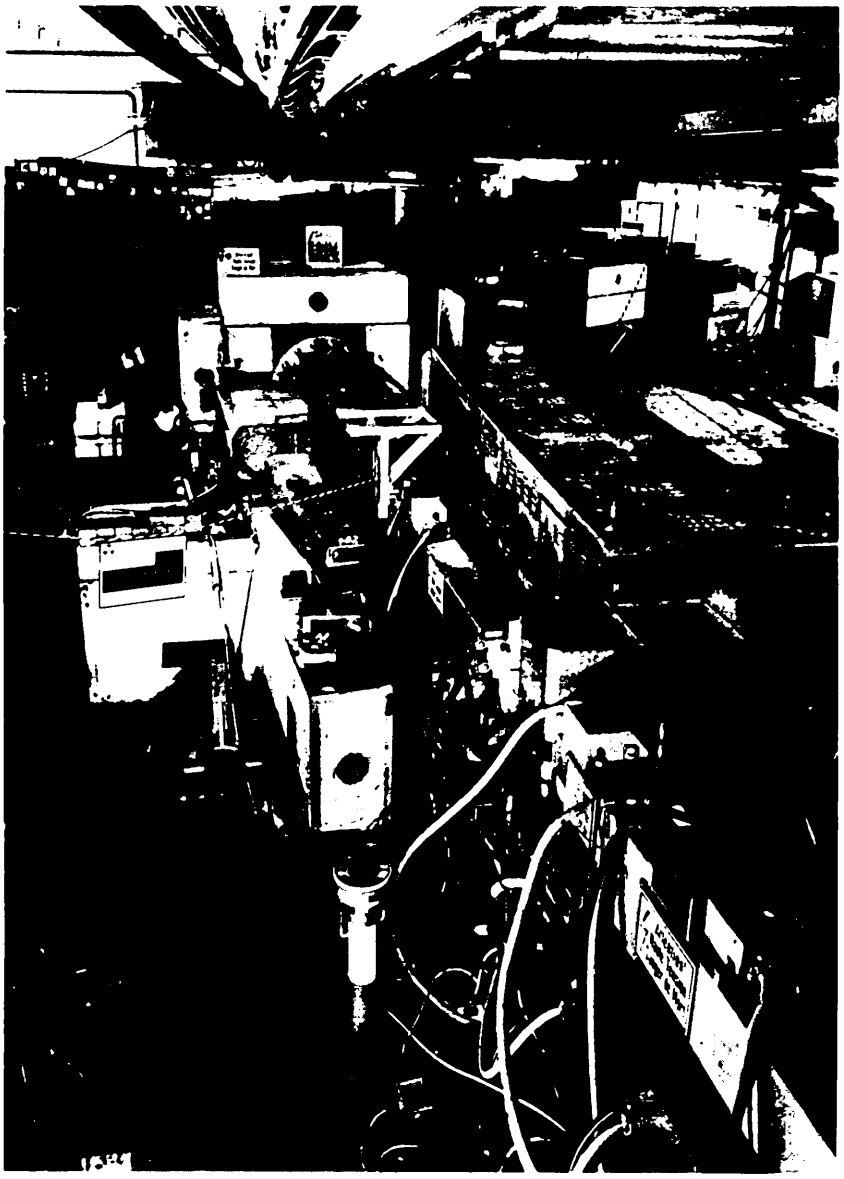

Fig. 32 View of the installed external proton beam

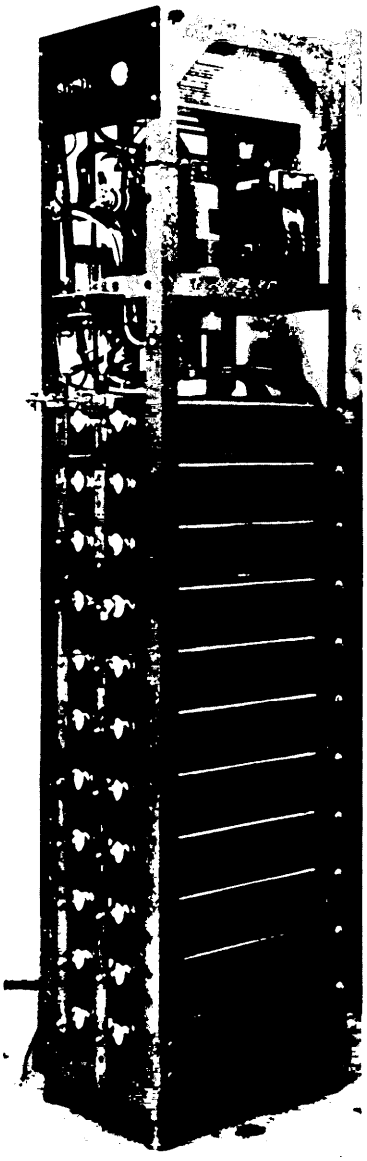

Fig. 33 Pulser rack for the pulsed beam transport magnets, showing the capacitors and, above them, the saturable reactor and one ignitron